2021

The Quantitative Assessment of Pond Scum: An examination of the biogeochemistry of phosphorus cycling in the Belgrade lakes

Abbey M. Sykes
Colby College

The Quantitative Assessment of Pond Scum:

An examination of the biogeochemistry of phosphorus cycling in the Belgrade lakes

By Abbey M. Sykes

A Thesis Presented to the Department of Chemistry,
Colby College, Waterville, ME
In Partial Fulfillment of the Requirements for Graduation with Honors in Chemistry

Submitted May 2021

The Quantitative Assessment of Pond Scum:
An examination of the biogeochemistry of phosphorus cycling in the Belgrade lakes

By Abbey M. Sykes

Approved:

D. Whitney King, Senior Advisor to the President,
Dr. Frank and Theodora Miselis Professor of Chemistry

_____
Date

Denise Bruesewitz, Associate Professor of Environmental Studies

_____
Date

Benjamin Twining, Senior Research Scientist at Bigelow Laboratory for Ocean Sciences, Henry L. and Grace Doherty Vice President for Education

_____
Date

TABLE OF CONTENTS

VITAE

Abbey May Sykes was born in Boston, Massachusetts on March 29, 1999 to Tracy and Kathleen Sykes. She grew up in Sudbury, Massachusetts, spending two years in Los Gatos, California, and graduated from Lincoln Sudbury Regional High School in 2017. Abbey was accepted by Colby College as a member of the class of 2021 where she began working in the King Lab during January of her first year. Over the past four years, Abbey has worked on several water quality research projects in the Belgrade Lakes Watershed of Central Maine under the supervision of Professor D. Whitney King. In March 2021, she participated in the Maine Sustainability and Water Conference hosted by the University of Maine at Orono where she was awarded first place in the Senator George J. Mitchell Center for Sustainability Solutions Undergraduate Student Poster Competition. Outside of Colby, Abbey spent a summer as a research technician in the Serhan Lab at Brigham and Women's Hospital/Harvard Medical School where she worked to identify the novel biological actions of 4,5-RCTR1 in planarian tissue regeneration under the supervision of Dr. Charles N. Serhan. Abbey was recently recognized as the winner of the Colby College Chemistry Department's ACS Division of Analytical Chemistry Award. Beyond her research endeavors, Abbey has been a chemistry tutor for three years, and has worked as an intern at several Boston-based non-profit organizations including CommonWealth Kitchen in Dorchester, MA and The Food Project in Lincoln, MA. Abbey will be graduating from Colby College in May 2021, earning her Bachelor of Arts degree in Chemistry with a concentration in Biochemistry. She will be moving on from Colby to return to the Serhan Lab in Boston, MA for a few years before pursuing further education.

LIST OF FIGURES

LIST OF TABLES

ABSTRACT

The internal recycling phosphorus in freshwater lake bottom sediments represents a significant source of hypolimnetic phosphorus (P) release for many of Maine's lakes. In summer months, Maine lakes often thermally stratify and the lake hypolimnion develops anoxia, leading to a reduction in redox potential at the sediment-water interface. These reducing conditions facilitate the reductive dissolution of ferric iron, and, since phosphorus is often present in freshwater lake sediments as solid $FeOOH\text{-}PO_4$ complexes, results in release of soluble phosphorus into the water column. Our current study presents field and laboratory data from sediment fractionation extractions designed to quantify concentrations of iron, aluminum and phosphorus in lake bottom sediments from East Pond (Smithfield, ME), Great Pond (Belgrade, ME) and China Lake (China, ME). We focus on elucidating the chemical foundations of the fractionation method so as to streamline our extraction procedure and minimize the required sample size. We confirm that internal P flux is negligible during hypolimnetic anoxia if molar Al:Fe is > 3. We ultimately hope to apply our extraction data to optimize aluminum dosing schemes designed to mitigate internal P flux in lakes above their phosphorus sorption threshold using the designated Al:Fe > 3 as an operational target for aluminum additions.

INTRODUCTION

1 The importance of Maine's lake industry to the state economy

Maine lakes are an invaluable resource to the state economy as they offer a low-cost source of drinking water, maintain lakeshore property values, boost the economic status of adjacent communities and contribute to the overall aesthetic appeal of life in Maine (The Economics of Lakes). Over the past few decades, studies conducted by the Maine Department of Environmental Protection have indicated that economic losses due to degrading water quality are an imminent threat to the quality of Maine life (The Economics of Lakes). In recent years, the water quality of many Maine lakes such as those in the Belgrade Lakes Watershed of Central Maine has declined due to increased instances of cyanobacterial blooms (high algal cell densities). In Maine lakes, these blooms not only adversely affect recreational aesthetics, but they may also introduce taste or odor issues in lakes used for drinking water or, if the blooms involve toxin-producing species, they may pose a serious threat to the health of animals and humans who interact with the lake (Madore, 2020).

2 Phosphorus is the limiting reagent in Maine lakes

Phytoplankton play a crucial role in maintaining the trophic status of freshwater lake systems as they are primary producers in the pelagic lake system food web. In the presence of excess nutrients, such as nitrogen (N) and phosphorus, algal populations grow rapi, leading todly blooms in the lake. The Redfield stoichiometry (equation 1) represents the average conserved ratio of biological nutrients in systems such as freshwater Maine lakes (Ptacnik et al., 2010). From this equation, we can understand the ecological stoichiometry of plant life in these lakes.

Redfield equation:

$$106\,CO_2 + 16\,NO_3^- + 1\,PO_4^{3-} + 122\,H_2O \rightarrow 1\,(CH_2O)_{106}(NH_3)_{16}(H_3PO_4) + 138O_2 \qquad (1)$$

As some cyanobacteria in Maine lakes are able to fix nitrogen from the atmosphere, we conclude that phosphorus is often the limiting nutrient involved in the growth of algal blooms (Schindler, 1977; Figure 1). Thus, it is critical to understand the biogeochemical basis of phosphorus cycling in freshwater lake systems in order to develop effective water quality management schemes.

Figure 1. Aerial images were taken by airplane over North Pond in Smithfield, ME during the summer of 2020; [left] algal blooms on North Pond, [P] = 30 ppb; [right] Little North Pond in a mesotrophic trophic state, [P] = 20 ppb.

2.1 Phosphorus flux in freshwater lake systems

There are two general processes for P flux into freshwater lakes: external loading and internal loading.

External loading

External nutrient loading is a pervasive issue in water quality management around the world (Song et al., 2017). While nutrients are essential for plant growth, an overabundance of nutrients in freshwater lake systems may lead to detrimental health and environmental effects such as

instances of algal blooming. The two most important nutrients that limit phytoplankton are phosphorus and nitrogen. Nitrogen occurs as ammonium (NH_4^+) or nitrate (NO_3^-), and phosphorus occurs as phosphate (PO_4^{3-}) or phosphate-containing molecules. As was forementioned, many aquatic plant species and phytoplankton in Maine lakes are able to fix nitrogen. As a result, the majority of water quality management schemes are focused largely on mitigating external phosphorus loading.

Excessive phosphorus inflow may be introduced via external loading from watershed runoff, groundwater incorporation, soil erosion, wildlife activity, man-made pollutants and discharges, and atmospheric systems. The majority of external phosphorus load has been reported to come from managed farmland and shoreline development (Phosphorus Control Action Plan: Echo Lake). Mitigating the external nutrient load of lake systems has been a widely accepted water quality management strategy.

The soil map depicted in Figure 2 describes the broad soil classification in the Belgrade Lakes Watershed. These soils all have the moderate potential to contribute to external phosphorus inflow upon erosion. Maine soils have formed via podzolization, gleization and formation of organic soils in the centuries since the last glacier in Maine melted over 12,500 years ago (Ferwerda et al., 1997). The primary soil types in this region, 5 and 7, are loamy tills largely derived from schist, granite, phyllite and gneiss (Ferwerda et al., 1997; Figure 2). This soil type constitutes approximately 23 percent of land area in Maine, including regions of the Belgrade Lakes where there is a significant slope near the lake (Ferwerda et al., 1997). Additional soil types to note include 15, sandy or gravelly glaciofluvial material derived mainly from slate, shale, phyllite, granite, gneiss and limestone, and 17, clayey or loamy glaciomarine or glaciolacustrine sediments mixed with loamy till (Ferwerda et al., 1997; Figure 2). Soil types 15

and 17 are both highly prone to erosion (Ferwerda et al., 1997). In contrast however, they are also often found in areas of little to no slope such as the peat bogs on North Pond, East Pond, Great Pond, Long Pond and Messalonksee lake (Wagner, personal communication). Soil types 5 and 7 have relatively organic carbon content as compared to types 15 and 17 (Ferwerda et al., 1997).

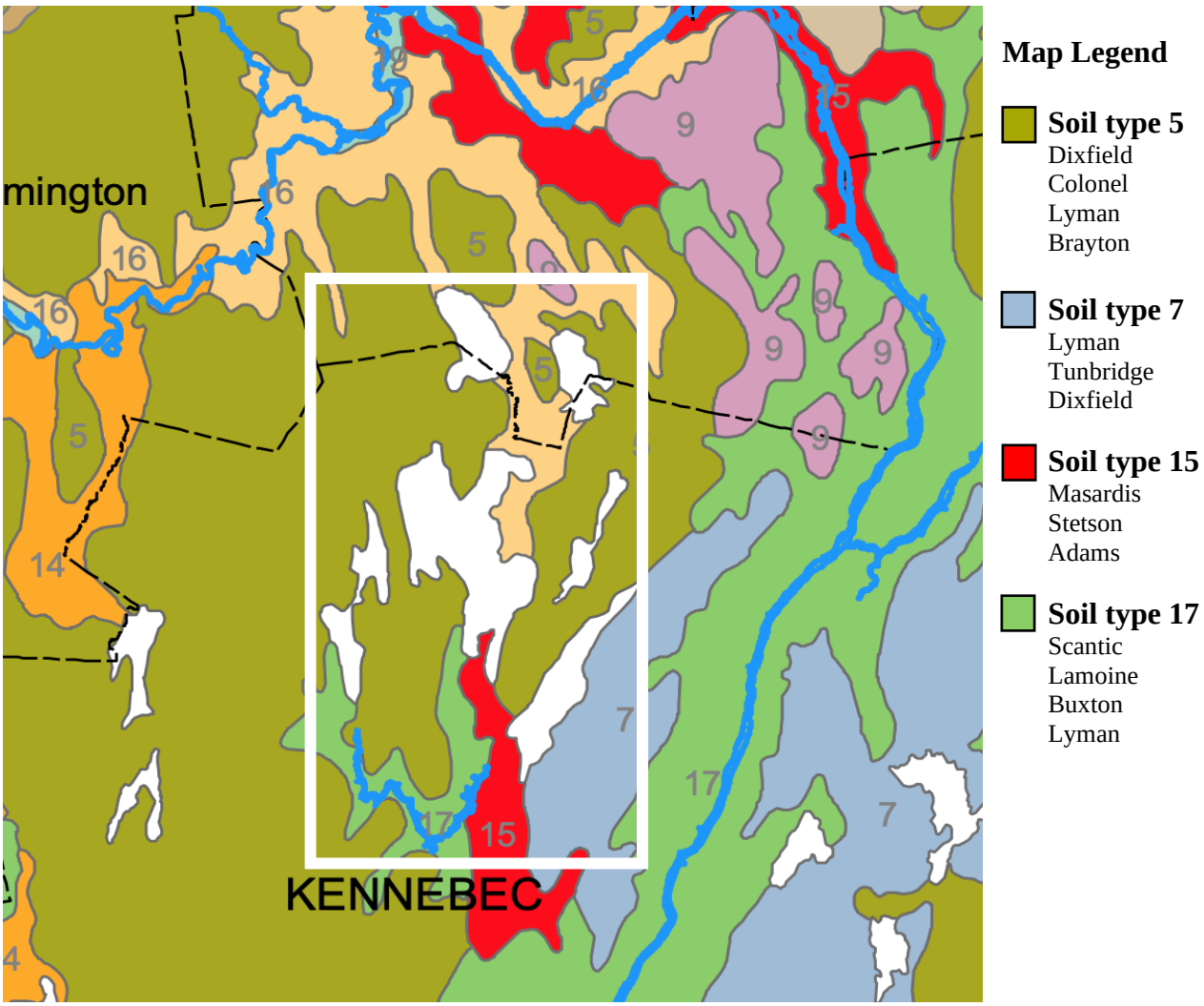

Figure 2. Soil map of the Belgrade Lakes Watershed (Ferwerda et al., 1997). Map legend refers to the four primary types of soil in the Belgrade Lakes Watershed and their general regions by town. The Belgrade Lakes Watershed is marked by the white box.

Internal loading

As the much of the soil in the Belgrade Lakes Watershed is highly susceptible to erosion, these lakes are candidates for excessive internal phosphorus loading as a result of historically high external load from sediment erosion. Historical excesses of external phosphorus load result in the accumulation of phosphorus rich organic material in the sediments of lakes. Oxidation of this organic material leads to release of phosphorus as phosphate to sediment pore waters where it binds to inorganic solid phases like iron and aluminum oxides. Excessive accumulation of dissolved organic carbon (DOC) in the hypolimnion also fuels sediment and bottom water anoxia and the subsequent reductive dissolution of phosphorus from the sediments, also known as the internal phosphorus load.

3 Lake management strategies

Ideally, in order to mitigate instances of algal blooming and revive the water quality of many Maine lakes, we could simply reduce the external load. This would involve riparian buffers, erosion control efforts, building runoff diversion ditches and introducing "light on land" forestry equipment, among others (Phosphorus Control Action Plan: Echo Lake). However, more recent analysis of P flux in the Belgrade Lakes concluded that controlling external phosphorus load alone is not an optimal management strategy because the primary source of phosphorus in some Maine lakes is internal recycling of the lake bottom sediments (Wagner, personal communication). Previous studies have reported that, while external loading is the dominant source of phosphorus in lakes, the temporal nature of internal phosphorus loading is often what leads to a dramatic increase in algal blooming during the summer months (Song et al., 2017). Thus, the internal recycling of phosphorus from lake bottom sediments can contribute

significantly to the overall P budget of a lake during the open water periods, and ultimately delay the lake's recovery from eutrophication for decades.

Empirically, we know that solid-phase aluminum (III) (Al^{III}) reduces the reductive dissolution of phosphorus from lake bottom sediments. The engineers who design aluminum treatments for blooming lakes simply add Al^{III} to lakes until internal loading is reduced, but often don't investigate the natural basis for the presence or absence of internal load.

This thesis looks at the chemical basis of internal loading and how the biogeochemistry of both iron and aluminum affects the rate and magnitude of phosphorus release. Our goal is to shift empirical measurements towards a more chemically robust analysis of phosphorus cycling that includes iron and aluminum geochemistry.

4 Iron and Aluminum speciation chemistry

In oxygenated water, the stable oxidation states of iron and aluminum are Fe^{III} and Al^{III}, respectively. The solubility of both iron and aluminum in the water column of freshwater lake systems at equilibrium is highly dependent on the pH of the solution.

Iron in aqueous solution may undergo hydrolysis, forming ferric hydroxides which influence iron solubility. In most (if not all) Maine lakes, the pH is not low enough to prevent iron tetrahydroxide formation, thus the majority of iron in oxygenated water is present as insoluble ferric hydroxide, $Fe(OH)_3$ (s).

The solubility of iron as iron hydroxide can be described by equation 2:

$$K_{sp} = [Fe^{3+}][OH^-]^3 \qquad (2)$$

The pH of solution affects Fe^{III} solubility directly due to the dependence of the hydroxide ion, but also indirectly by changing Fe^{3+} activity via the formation of iron hydroxide complexes.

Thus, it is critical to understand the pH-dependent iron species in freshwater lake systems. Hydroxide is added to ferric iron forming soluble, sequential iron hydroxide species.

$$Fe^{3+} + OH^- \overset{\beta 1}{\Leftrightarrow} FeOH^{2+} \qquad (3)$$

$$Fe^{3+} + 2OH^- \overset{\beta 2}{\Leftrightarrow} Fe(OH)_2^+ \qquad (4)$$

$$Fe^{3+} + 3OH^- \overset{\beta 3}{\Leftrightarrow} Fe(OH)_3 \qquad (5)$$

$$Fe^{3+} + 4OH^- \overset{\beta 4}{\Leftrightarrow} Fe(OH)_4^- \qquad (6)$$

The total iron in the lake is thus described by:

$$T_{Fe} = [Fe^{3+}] + [FeOH^{2+}] + [Fe(OH)_2^+] + [Fe(OH)_3] + [Fe(OH)_4^-] \qquad (7)$$

So, the fraction of each iron species is described by α:

$$\alpha_n = \frac{[n]}{T_{Fe}} \qquad (8)$$

where *n* represents each species. For ferric iron,

$$\alpha_0 = \frac{[Fe^{3+}]}{T_{Fe}} \qquad (9)$$

The definition of α_0 can be further defined using the equilibrium constants for the complexation of iron hydroxides (see Table 1):

$$\alpha_0 = \frac{[Fe^{3+}]}{[Fe^{3+}] + [FeOH^{2+}] + [Fe(OH)_2^+] + \cdots} \qquad (10)$$

$$\alpha_0 = \frac{Fe^{3+}}{Fe^{3+} + \beta 1 \cdot Fe^{3+}[OH^-] + \beta 2 \cdot Fe^{3+}[OH^-]^2 + \cdots} \qquad (11)$$

$$\alpha_0 = \frac{1}{1 + \beta 1 \cdot [OH^-] + \beta 2 \cdot [OH^-]^2 + \cdots} \qquad (12)$$

We can now express the solubility of ferric iron in terms of total iron by combining equations 2 and 9:

$$K_{sp} = [Fe^{3+}][OH^-]^3 = \alpha_0 \cdot T_{Fe} \cdot [OH^-]^3 \qquad (13)$$

The above series of equations details the solubility of iron in freshwater lakes. Figure 3 demonstrates the solubility of Fe^{III} species in solution as a function of pH.

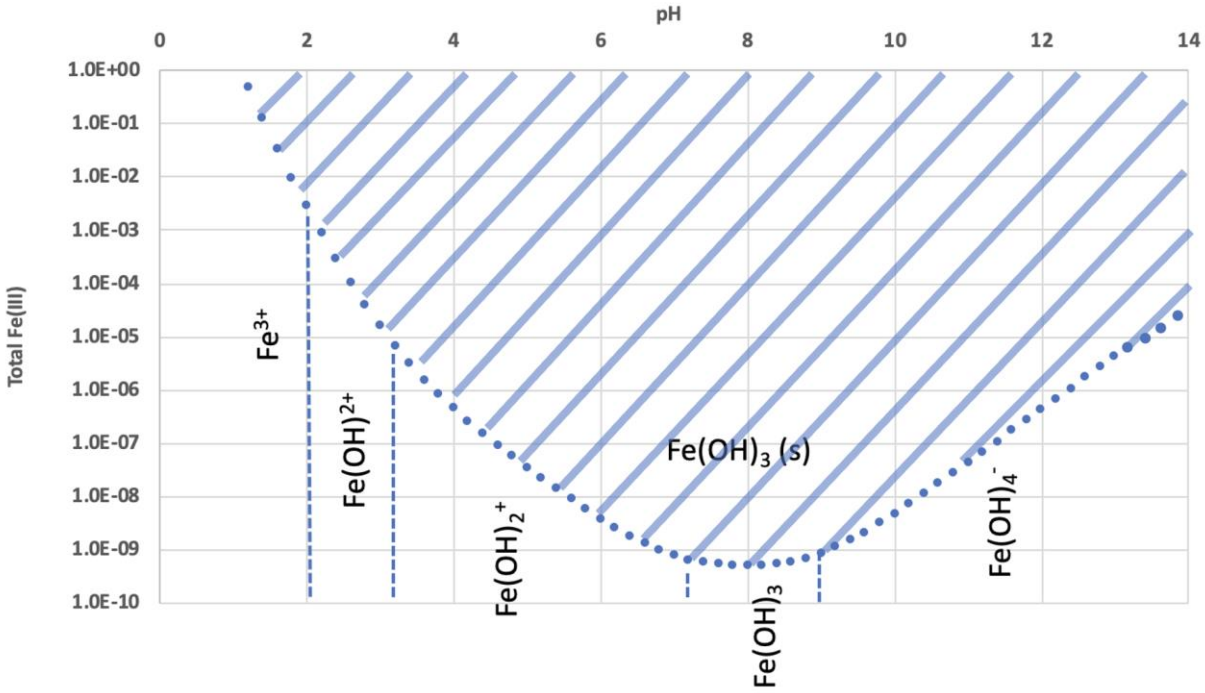

Figure 3. Fe^{III} speciation and solubility in pure water as a function of pH. Solubility in moles/liter.

Figure 3 demonstrates that the solubility of Fe^{III} decreases with increasing pH, reaching a minimum around 1 nM at pH 7. As the solution becomes more basic, iron solubility begins to increase as Fe^{III} solution phase complexes, $Fe(OH)_4^-$, become more abundant.

The same fundamental behavior applies to the solubility chemistry of aluminum, just with different equilibrium constants (Table 1). Figure 4 demonstrates pH-dependent aluminum speciation following the same approach we used to calculated pH-dependent iron speciation. As with Fe^{III} (Figure 3), the observed solubility of Al^{III} reaches a minimum around pH 7 (Figure 4). This is important to note as both metals reach their solubility minima at the natural pH of lake water.

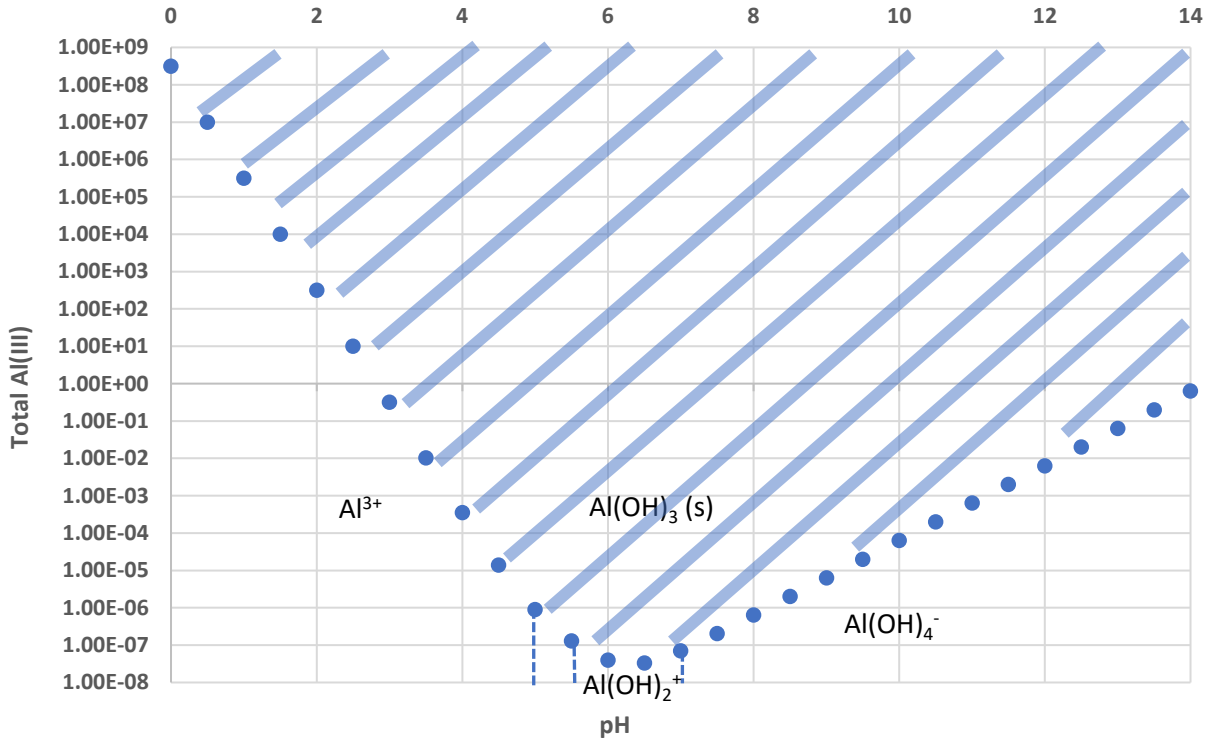

Figure 4. Al^{III} speciation and solubility in pure water as a function of pH. Solubility in moles/liter.

Table 1. Standard K values for critical iron and aluminum species generated in ChemEql (Stumm & Morgan, 1996; Smith & Martell, 1989).

	Species	K
Fe	Fe^{++}	13.0
	$FeOH^{++}$	-2.2
	$Fe(OH)_2^{+}$	-5.7
	$FeOH^{+}$	-9.5
	Fe^{+++}	-13.0
	$Fe(OH)_2$ (aq)	-20.6
	$Fe(OH)_3$ (aq)	-25.6
	$Fe(OH)_3^{-}$	-32.0
	$Fe(OH)_4^{-}$	-34.6
	$Fe(OH)_4^{--}$	-46.4
Al	Al^{+++}	10.8
	$Al(OH)^{++}$	5.8
	$Al(OH)_2^{+}$	0.7
	$Al(OH)_3$ (aq)	-6.1
	$Al(OH)_4^{-}$	-14

5 Iron and aluminum as solid phase adsorbents for phosphorus

In their solid phases, both iron and aluminum adsorb phosphorus as phosphate in a well-oxygenated environment (Kopácek et al., 2005). Thus, the P flux is controlled by the abiotic complexation of phosphate by Fe^{III} and Al^{III}:

$$\equiv FeOH_2^{+} + H_2PO_4^{-} \rightarrow \equiv FeOH_4PO_4 \qquad (14)$$

$$\equiv AlOH_2^{+} + H_2PO_4^{-} \rightarrow \equiv AlOH_4PO_4 \qquad (15)$$

To model this chemistry, we need to consider the acid/base chemistry of both metals and phosphate. We know that phosphorus as phosphate has three protonated states in solution:

$$H_3PO_4 \overset{k_1}{\Leftrightarrow} H^+ + H_2PO_4^- \qquad (16)$$

$$H_2PO_4^- \overset{k_2}{\Leftrightarrow} H^+ + HPO_4^{2-} \qquad (17)$$

$$HPO_4^{2-} \overset{k_3}{\Leftrightarrow} H^+ + PO_4^{3-} \qquad (18)$$

However, in considering the acid/base properties of phosphate, we know that only the second protonation state and acidity constant are important in a pH range of 5-9 (the range most applicable to biological freshwater lake systems). As such, the fraction of each phosphate species relative to total phosphorus can be described as follows:

$$\alpha_0 = \frac{[H_3PO_4]}{Total\ P}, \alpha_1 = \frac{[H_2PO_4^-]}{Total\ P}, \alpha_2 = \frac{[HPO_4^{2-}]}{Total\ P}, \alpha_3 = \frac{[PO_4^{3-}]}{Total\ P} \qquad (19)$$

We then extrapolated the speciation further to incorporate the acid dissociation constants (Appendix A) associated with each deprotonation, and arrived at the following:

$$\alpha_0 = \frac{[H^+]^3}{d}, \alpha_1 = \frac{k_1[H^+]^2}{d}, \alpha_2 = \frac{k_1k_2[H^+]}{d}, \alpha_3 = \frac{k_1k_2k_3}{d} \qquad (20)$$

Where,

$$d = [H^+]^3 + k_1[H^+]^2 + k_1k_2[H^+] + k_1k_2k_3 \qquad (21)$$

Using the same mathematical basis, we defined the speciation for iron oxides:

$$\equiv FeOH_2^+ \overset{k_1}{\Leftrightarrow} H^+ + \equiv FeOH \qquad (22)$$

$$\equiv FeOH \overset{k_2}{\Leftrightarrow} H^+ + \equiv FeO^- \qquad (23)$$

Total solid iron is defined as:

$$T_{Fe} \equiv FeOH_2^+ + \equiv FeOH + \equiv FeO^- \qquad (24)$$

It is important to note that equations 22-24 define the acid/base properties of the Fe^{III} solid phase which is a different chemical species than Fe^{III} solution phase complexes. The adsorption of phosphorus as phosphate to $FeOH_2^+$ as described by equation 14 can thus be defined as:

$$K_{Fe} = \frac{[\equiv FeOH_3PO_4^-]}{[\equiv FeOH_2^+][HPO_4^{2-}]} = \frac{[\equiv FeOH_3PO_4^-]}{[\alpha_{0,Fe} * T_{Fe}][\alpha_{2,P} * T_P]} \qquad (25)$$

Similarly, K'_{Fe} can be defined as:

$$K'_{Fe} = K_{Fe}\alpha_{0,Fe}\alpha_{2,P} = \frac{[\equiv FeOH_3PO_4^-]}{[T_{Fe}][T_P]} \qquad (26)$$

The fraction of phosphorus adsorbed to iron is:

$$Fraction\ P\ adsorbed\ to\ Fe(III) = \frac{K_{Fe}\alpha_{0,Fe}\alpha_{2,P}[T_{Fe}][T_P]}{1 + K_{Fe}\alpha_{0,Fe}\alpha_{2,P}[T_{Fe}][T_P]} \qquad (27)$$

Equation 27 is described by Figure 5. Figure 5 demonstrates the fraction of dissolved $H_2PO_4^-$ in stream water as a function of pH. As pH increases, the fraction of phosphorus as phosphate adsorbed to Fe^{III} decreases and thus the dissolved fraction of $H_2PO_4^-$ increases.

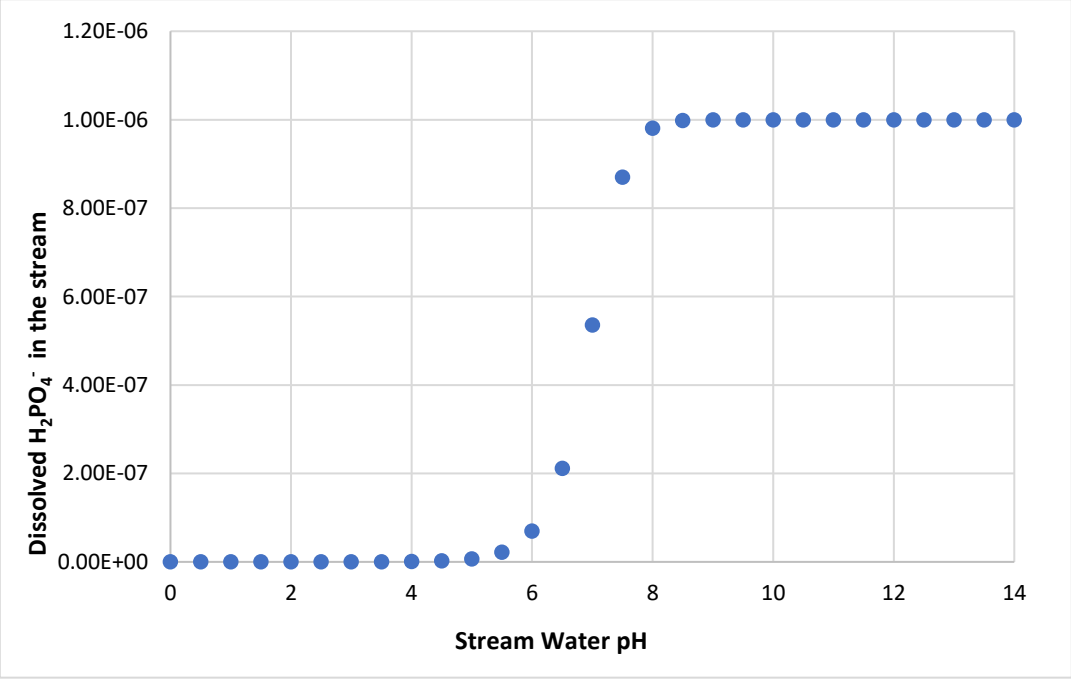

Figure 5. Calculated adsorption edge for $H_2PO_4^-$ in sediments as a function of pH. (Note: stream water and lake water are chemically identical (King, personal communication).)

The same is true of aluminum oxide adsorption of phosphorus as phosphate:

$$K'_{Al} = K_{Al}\alpha_{0,Al}\alpha_{2,P} = \frac{[\equiv AlOH_3PO_4^-]}{[T_{Al}][T_P]} \qquad (28)$$

Both $\equiv FeOH_2^+$ and $\equiv AlOH_2^+$ are in competition for $H_2PO_4^-$. Thus, the fraction of phosphate adsorbed by aluminum may be described as the ratio of these apparent K' binding constants and total concentrations of solid-phase metal:

$$Fraction\ of\ P\ adsorbed\ to\ Al(III) = \frac{K'_{Al}T_{Al}}{K'_{Al}T_{Al} + K'_{Fe}T_{Fe}} \qquad (29)$$

Mass conservation requires that the fraction of phosphorus adsorbed to Fe^{III} be 1-faction adsorbed by Al^{III}. The resultant plot from this model is given in Figure 6. Note that as molar Al:Fe increases (i.e., there is increasingly more aluminum in solution than iron), the fraction of phosphorus adsorbed by Fe^{III} decreases. While phosphorus adsorption modeling gives us insight into the competitive affinity of iron versus aluminum for phosphate binding, it neglects to tell us anything about the chemical kinetics of phosphate adsorption. We return to the discussion of kinetics at the end of this thesis.

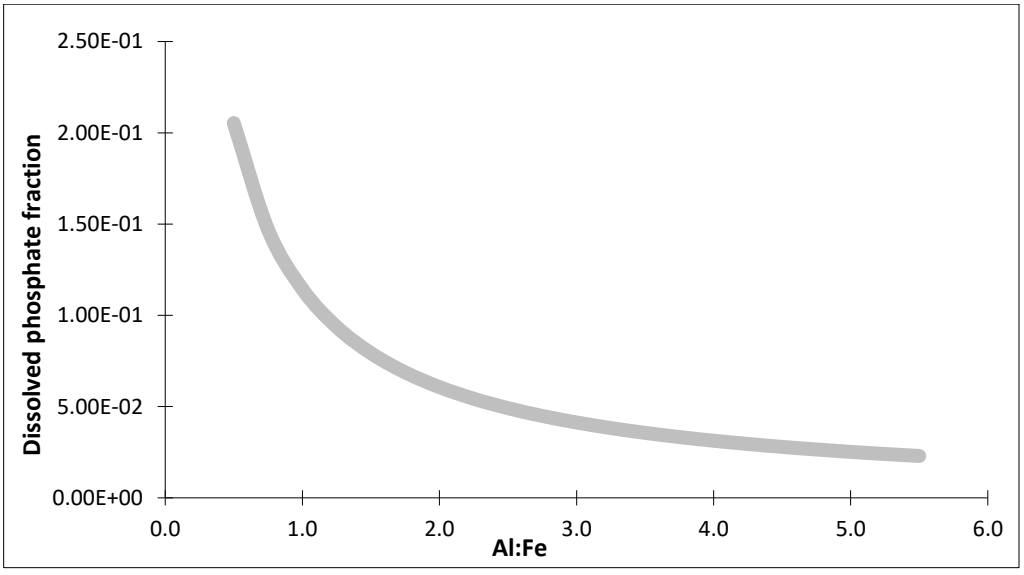

Figure 6. Adsorption model for phosphorus as phosphate binding to aluminum as a function of Al:Fe.

6 Iron and aluminum redox chemistry

When levels of organic carbon are increased in lake bottom sediments, the redox conditions change as a result. We must also consider how iron and aluminum change in sediments as redox conditions change.

6.1 Role of organic material in freshwater systems

Organic material in lake sediments plays a large role in internal P flux. As organic material reaches the sediment-water interface, it is oxidized by a variety of respiratory processes that rely on different electron acceptors such as oxygen (O_2), nitrate (NO_3^-), sulfate (SO_4^{2-}), Mn oxides and Fe oxides. The oxidation of organic carbon (C_{org}) has a significant impact on the release of sediment-bound phosphorus if redox conditions change. Certain electron acceptors such as O_2, NO_3^- and Mn^{IV} are more easily reduced and will thus be consumed by organic carbon oxidation first (Figure 7).

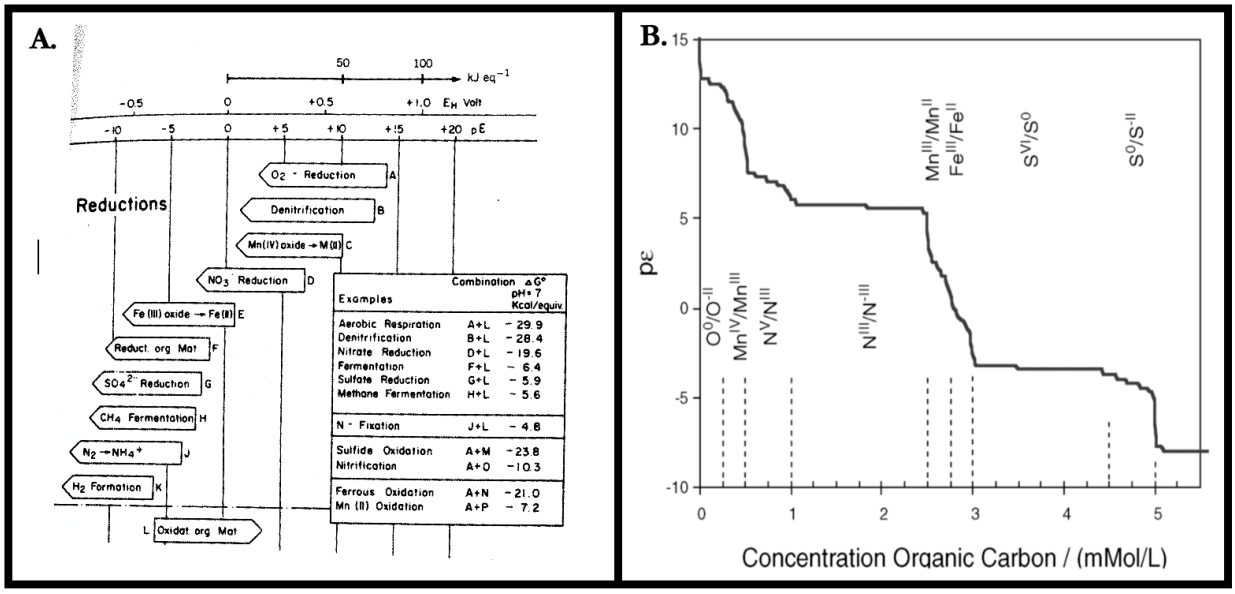

Figure 7. Redox chemistry of organic carbon and electron-accepting species found in freshwater lake sediments; [A] relative reduction potentials of prominent reducible species (O_2, Mn^{IV}, NO_3, Fe^{III}, SO_4^{2-}) in freshwater lake bottom sediments (Stumm, 1996); [B] predicted titration curve for the reduction of prominent sediment-bound elements (O, Mn, N, Fe, S) by organic carbon at pH 7 (King, 2002).

In lakes with low oxygen concentrations (hypoxia) and/or excess organic material, sediment bound Fe^{III} will eventually be reduced leading to the subsequent release of phosphorus as phosphate. When the supply of organic carbon is relatively higher than oxygen concentrations in freshwater lake systems, we see a change in the redox conditions of the lake. From Figure 7B, we see that as oxygen is depleted, the solution becomes more reducing. This is exactly what is happening at the sediment-water interface in anoxic lakes.

6.2 The reductive dissolution of ferric iron is responsible for phosphorus release

Phosphorus is primarily present in lake sediments in solid $FeOOH\text{-}PO_4$ or $AlOOH\text{-}PO_4$ complexes (equations 14 and 15) formed by the adsorption of phosphate to sediment-bound ferric iron (Gächter & Meyer, 1993). This is because both Fe^{III} and Al^{III} have strong binding capacities for inorganic phosphate under oxic conditions (Lake et al., 2007). However, as Fe^{III}-reducing microbial activity thrives in an anoxic environment, Fe^{III} is reduced to Fe^{II}, ultimately releasing phosphate and distributing Fe^{II} and phosphorus into the water column (Lake et al., 2007). Figure 8 represents a simplified schematic for an impacted lake versus a pristine lake. Note that the increased flux of phosphorus upon reduction of Fe^{III} to Fe^{II} promotes algal blooming. Since it is impractical to physically remove phosphorus from lakes, water quality management schemes must incorporate a way to “lock” it into the sediments in order to mitigate reductive phosphorus release.

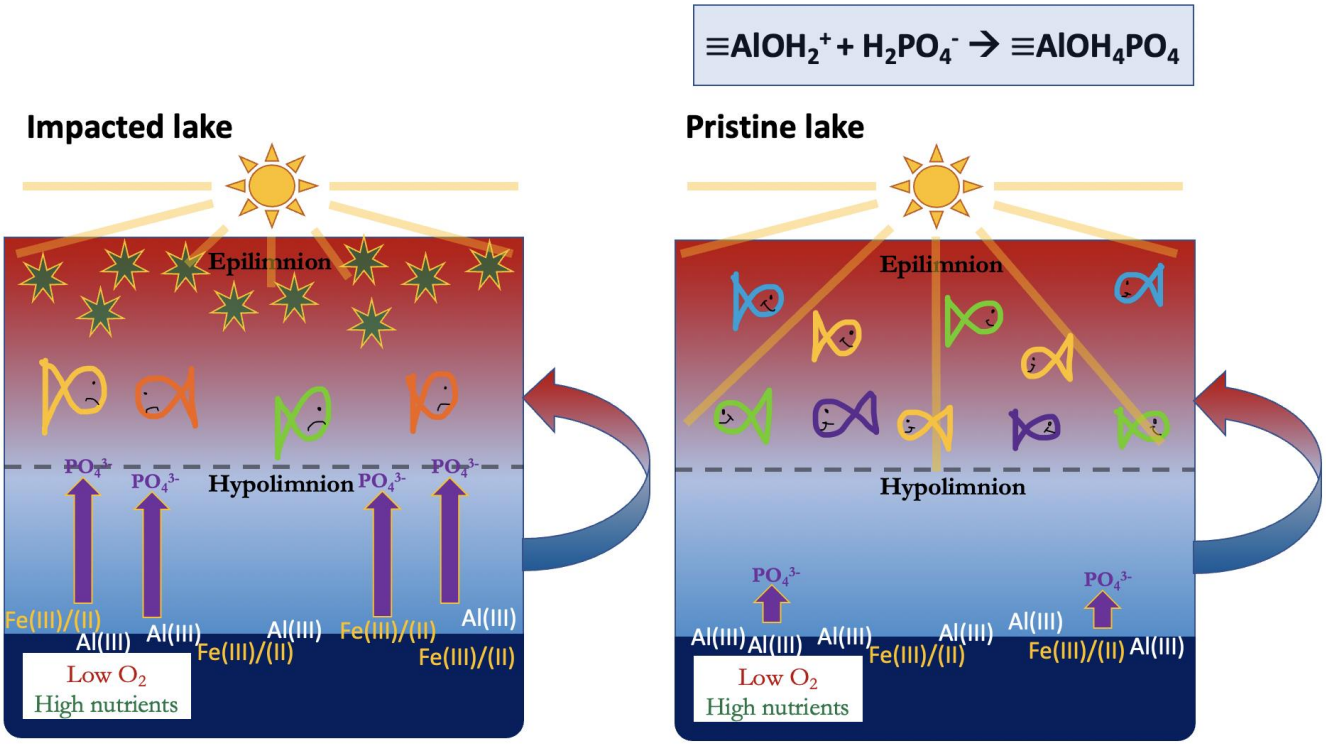

Figure 8. Schematic for phosphorus release as phosphate in an impacted lake (left) and a pristine lake (right).

Lake managers ultimately turn to aluminum as a tool to lock phosphorus released from reduced iron into lake bottom sediments. However, it is critical that we first understand the chemical redox relationships between iron, aluminum and phosphate.

Iron, relatively abundant in the composition of the Earth's crust, occurs in two primary oxidation states: divalent (or ferrous) Fe^{++} and trivalent (or ferric) Fe^{+++} (Hem, 1962). As such, iron in aqueous solution such as lake water systems is subject to pH (as described in section 4) and redox potential (pE) dependent hydrolysis. There are several important ionic iron species including Fe^{+++}, $FeOH^{++}$, $Fe(OH)_2^{+}$, Fe^{++} and $FeOH^{+}$ (Hem, 1962). In most freshwater systems with a pH ranging between pH 5 and 8, iron hydroxides form naturally, precipitating iron most commonly as ferric hydroxide, or $Fe(OH)_3$ (Hem, 1962; Figure 3). Under conditions of chemical equilibrium in freshwater lake systems containing both divalent and trivalent iron species, the

redox potential is dependent on the relative abundance of reducing and oxidizing iron species present.

The transition between oxidized iron species and reduced iron species is related through the Nernst equation:

$$E = E^{\circ} + \frac{RT}{nF} lnQ \qquad (30)$$

in which Q represents the ratio of reduced species to oxidized species. For the ferrous-ferric system at 25ºC, this equation becomes:

$$E = E^{\circ} - 0.05916 + log \frac{[Fe^{2+}]}{[Fe^{3+}]} \qquad (31)$$

Using T_{Fe} and α_n defined by equations 7-9, we can express redox potential via the Nernst equation in terms of total iron:

$$E = E^{\circ} - 0.05916 + log \frac{T_{Fe(II)}\alpha_1}{T_{Fe(III)}\alpha_0} \qquad (32)$$

$$E' = E^{\circ} - 0.05916 + log \frac{\alpha_1}{\alpha_0} \qquad (33)$$

$$E = E' - 0.05916 + log \frac{T_{Fe(II)}}{T_{Fe(III)}} \qquad (34)$$

In concert with the pH-dependent speciation of iron and aluminum in freshwater lake systems, equations 30 through 34 can be applied to generate pE-pH diagrams that characterize the acid/base and redox chemistries of these molecules. Figure 9 shows Pourbaix plots, or pE-pH diagrams, for iron and aluminum species in freshwater lakes. The upper boundary represents the pE and pH of oxidized natural water while the lower boundary represents the pE and pH of reduced natural water.

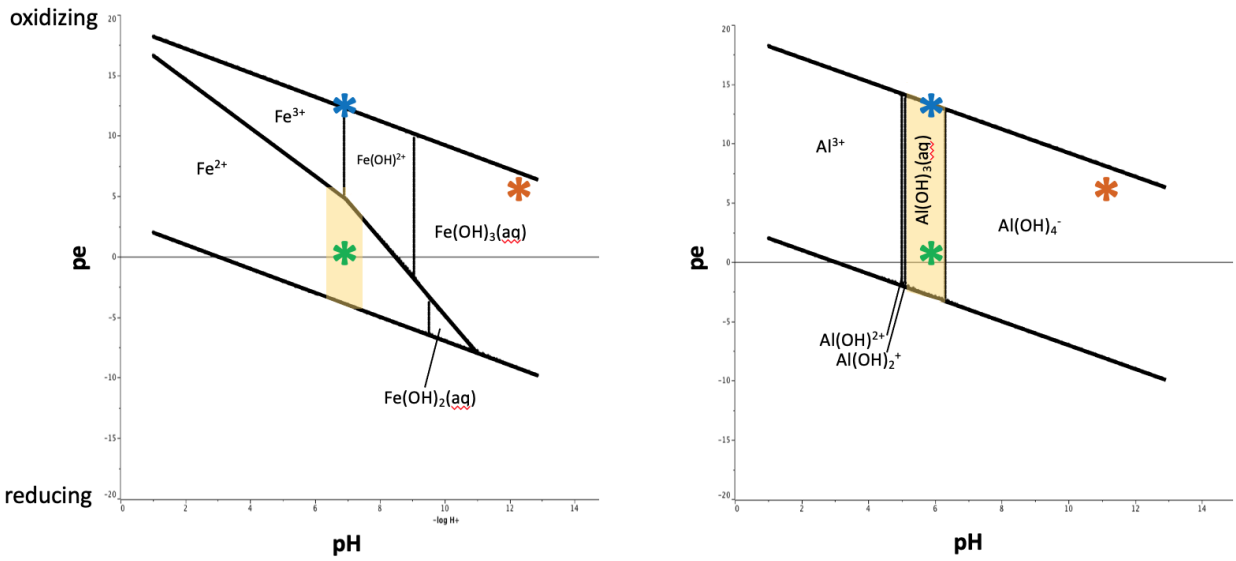

Figure 9. Pourbaix plots for iron (left) and aluminum (right) in water generated using ChemEql. Pure redox reactions are marked by the horizontal lines and pure acid-base reactions are marked by the vertical lines. The blue star represents iron and aluminum stable conditions in oxygenated pore water conditions; the green star represents iron and aluminum in high carbon, low oxygen conditions. The yellow box represents the potential range of the green star, depending on the amount of reducing agent required to fully reduce Fe^{III} to Fe^{II}.

If both Fe^{III} and Al^{III} were stable under all environmental conditions, our job would be done. Instead, we have to find a way to combat the reductive dissolution of phosphorus from iron under anoxic conditions. The Pourbaix diagrams for iron and aluminum clearly present the redox and acid/base capabilities of iron and aluminum as Lewis acids, allowing us to ultimately distinguish between the relative phosphate retention abilities of each Lewis acid. As is shown in Figure 9 by the lack of horizontal lines in the aluminum Pourbaix plot, aluminum species can only change with pH, not with pE. Thus, as aluminum has a single oxidation state (Al^{III}), Al^{III} is a more effective Lewis acid than Fe^{III} for the retention of phosphorus in lake bottom sediments because it cannot be reduced by organic carbon. It is also important to note that Fe^{II}, a third Lewis acid, is also present. While Fe^{II} is capable of binding phosphate, it is a much weaker

Lewis acid than Fe^{III} as the charge-to-size ratio is changed upon the reduction of Fe^{III} to Fe^{II}. Fe^{II} is also highly soluble at the natural pH of freshwater lakes.

7 Aluminum treatment as a way to combat internal phosphorus load

Like iron, aluminum enters the lakes from the sediments upon the weathering of terrestrial rocks and soils. Figures 3 and 4 suggest that Al^{III} is only about one order of magnitude more soluble than Fe^{III} in pure water at pH 7. While Al^{III} concentrations in the Belgrade lakes are below the inorganic solubility limit for amorphous aluminum hydroxide, Fe^{III} must be solubilized by other ligands in the lake bottom sediments (King, personal communication). Upon photooxidation of these organic ligands, the metal-ligand bonds are cleaved, releasing Fe^{III} and Al^{III} into the water column as $Fe(OH)_3$ (s) and $Al(OH)_3$ (s) (Porcal, 2010). Although both Fe^{III} and Al^{III} are naturally occurring metals known to decrease P flux in freshwater lake systems, the relative ability of Fe^{III} as compared to Al^{III} to bind phosphorus is dramatically hindered by its reduction under high organic carbon, low oxygen conditions. Thus, phosphorus retention strategies via complexation with Fe^{III} present an issue.

Previous studies have demonstrated considerably low rates of phosphorus sequestration by Al^{III} in lake sediments (Kopáček et al. 2000; 2001). Since Al^{III} is not susceptible to redox reactions, it is considered a permanent phosphorus sink in freshwater lake systems (Lake et al, 2007; Figure 9). As such, increasing the abundance of solid phase Al^{III} at the sediment-water interface via alum ($Al_2(SO_4)_3$) treatments has emerged as a viable lake management strategy to mitigate internal phosphorus loading in eutrophic lake systems.

8 Conventional "jar test" methods used to engineer aluminum dose

Classic "jar test" experiments are typically used as small-scale mesocosms in a laboratory setting to engineer alum treatments by measuring phosphorus released from anoxic sediments as a

function of redox-insensitive aluminum concentration. The majority of these jar test studies are empirical in nature as they focus only on measuring reductive phosphorus release in controlled circumstances.

8.1 East pond alum treatment

In 2018, East Pond in Smithfield, ME was experiencing algal blooms as a result of hypolimnetic anoxia and a buildup of organic carbon at the sediment-water interface. Figure 10 shows Secchi depth measurements in East Pond since 1975. From this plot it is clear that rapid changes in the chemistry of freshwater lake systems can have dramatic effects such as intense algal blooming.

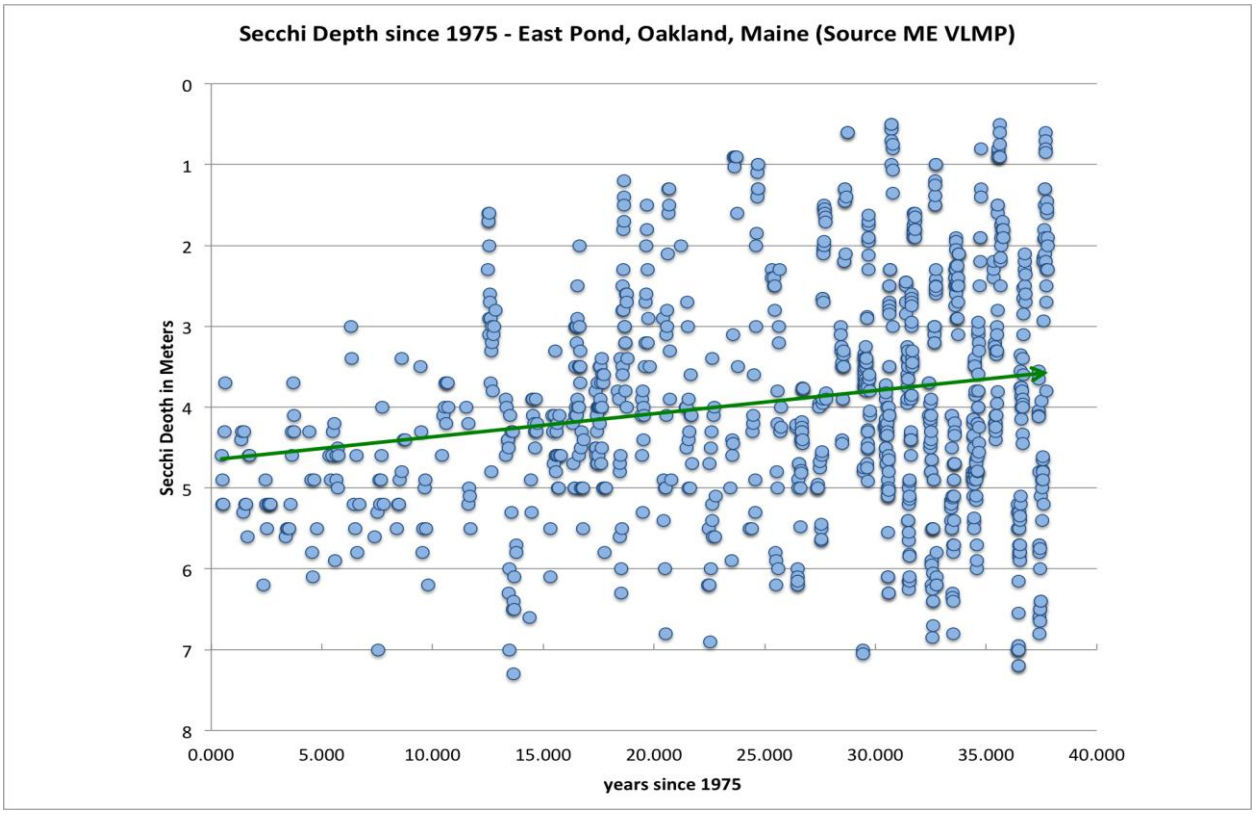

Figure 10. Secchi depth on East Pond since 1975 (Source ME VLMP). A lake is considered impacted when Secchi is less than two meters.

In order to mitigate algal blooming on East Pond, the King Lab at Colby College quantified reductive phosphorus release as a function of intentionally added aluminum in order to determine the optimal alum-dosing scheme. Typically, extraction procedures consist of five extraction

steps, however we used a slightly condensed version of the Psenner & Pucsko (1988) procedure that only focuses on three critical extraction steps. (1) 0.1 M ammonium chloride at room temperature (RT) to extract pore water and loosely bound iron, aluminum and phosphorus; (2) 0.11 M sodium bicarbonate ($NaHCO_3$)-buffered sodium dithionite ($Na_2S_2O_4$) at RT to extract reduced iron in sediment and associated phosphorus; (3) 0.1 M sodium hydroxide (NaOH) at RT to extract amorphous iron and aluminum hydroxides, and associated phosphorus. This study details an empirical fractionation procedure suitable to distinguish between a variety of chemically well-defined phosphorus compounds in freshwater sediments. The King Lab extraction scheme is laid out in Figure 11.

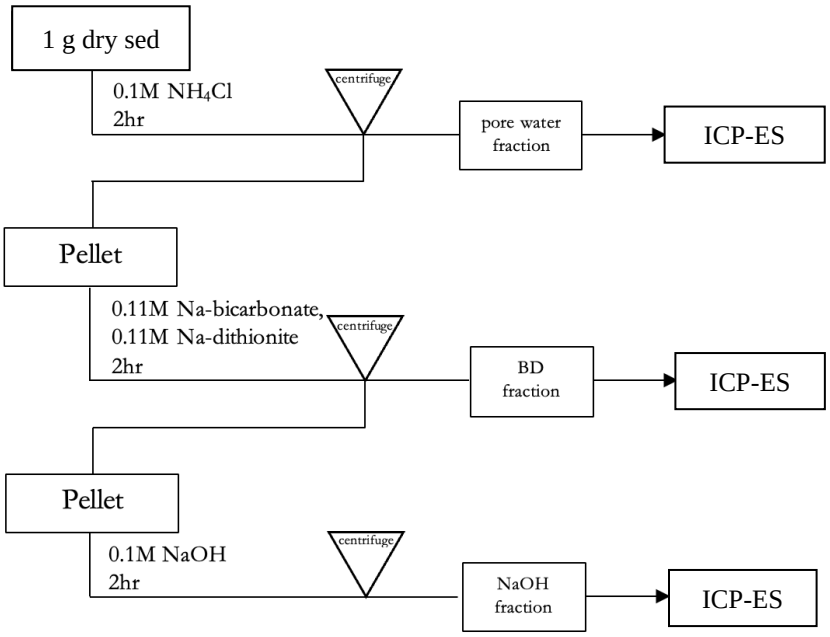

Figure 11. Schematic representation of phosphorus fractionation extraction procedure used to analyze iron, aluminum and phosphorus concentrations in East Pond sediment samples. See Appendices B and C for a more detailed procedure.

Raw extraction data from East Pond sediment samples were analyzed for reductive phosphorus release as a function of added aluminum. This data showed trends consistent with the

theory described above: reductive phosphorus release decreases as aluminum concentration increases (Appendix D; Figure 12).

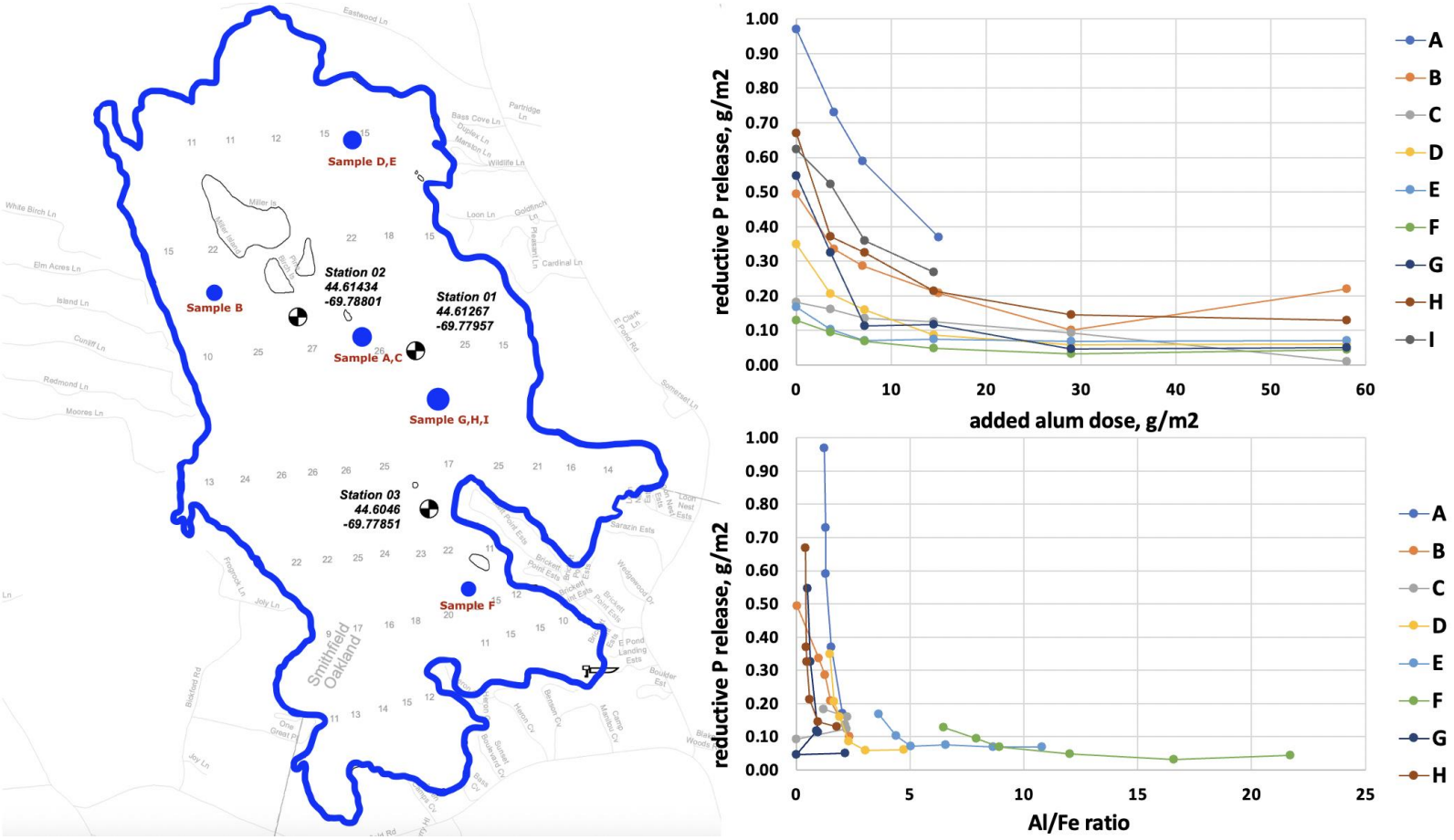

Figure 12. Sequential sediment extraction data from East Pond.

It was ultimately determined that East Pond should be treated with 45 g alum/m^2 in order to minimize reductive phosphorus release from lake bottom sediments. However, the East Pond sequential extractions were carried out prior to our current full understanding of the biogeochemistry of our extraction methodology. The primary area of uncertainty during the East Pond project was the role of our reducing reagent, sodium dithionite, and its chemical behavior. We have since characterized dithionite and its role in sediment extractions as will be discussed in the subsequent sections of this thesis. Similarly, during this study, we measured only reductive

phosphorus release, neglecting levels of both iron and aluminum. Despite this, more than two years after the initial alum treatment, East Pond remains clear and extraction analysis indicates low levels of phosphorus release upon reduction, indicating that the treatment was successful regardless of our error. Our recommendation for treatment dosage was likely more than enough aluminum to keep the phosphorus bound up in the sediments. Yet, the reproducibility of this experiment was weak; we now recognize that our analytical work was inefficient, and a better understanding of the chemistry will ultimately improve extraction reproducibility.

Therefore, before we move on to treat other Maine lakes with alum as we did for East Pond, it is important that we understand the chemical foundations of what is still a fairly empirical procedure. Historically, researchers have used the Psenner & Pucsko method strictly to analyze sedimentary concentrations of phosphorus, while neglecting to understand variation in iron and aluminum levels. We believe that characterizing the redox and acid/base chemistry of the traditional extraction method will better inform future alum dose engineering studies.

9 The aluminum to iron molar ratio

Recent literature on the biogeochemistry of phosphorus cycling in Maine lakes has shown that molar Al:Fe plays a major role in the release of phosphorus under reducing conditions (Norton, et al., 2008). Phosphorus adsorption is directly linked to the chemistry of Fe^{III} and Al^{III} in lake bottom sediments (Norton et al., 2008). Conventional jar tests empirically extract sediments by changing the pH and pE of extraction reagents (Figures 9 and 11). Separate from the jar test studies, geochemical analyses of phosphorus release provide foundational insight into the chemical relationship between iron and aluminum sediment concentrations and phosphorus release. Thus, we argue that the two approaches can be merged to develop a comprehensive chemical model for hypolimnetic phosphorus release in both natural and engineered freshwater

lake environments. Relevant literature has demonstrated that there is no need to add Al^{III} to lake systems in order to study the importance of Al^{III} on internal load as internal P flux is reduced during hypolimnetic anoxia if molar Al:Fe is > 3 (Kopáček et al., 2005). The 3:1 ratio indicates chemically stable levels of iron and aluminum are required to modulate P flux from sediments. This ratio can be applied as an operational target for estimating optimal aluminum dosing in freshwater lakes suffering from algal blooming. In other words, it is important to apply the empirical jar tests to well-defined chemical systems in order to fully understand the biogeochemistry of reductive phosphorus release. At the time of the East Pond alum treatment, we did not include analysis of Al:Fe in our final treatment recommendation. However, it appears that the East Pond alum treatment successfully improved water clarity, so we went back to our raw extraction data to look at the iron and aluminum levels in each sample. We ultimately found that, despite our oversight, the 45 g/m^2 recommended alum dose was enough aluminum to push Al:Fe of East Pond from 1:1 to 3:1. Thus, the goal of this current work is to tie all of these processes together into a comprehensive model for studying phosphorus release in freshwater lakes.

10 Characterization of the reductive step in the Psenner & Pucsko method

An important place to start is to consider the chemistry of dithionite, used as a redox buffer in the reductive extraction step (Figure 8). This step is the primary area of analytical uncertainty in the traditional jar test method. As was forementioned, freshwater lake scientists have largely adopted the extraction procedure of Psenner & Pucsko (1988) to analyze sedimentary concentrations of phosphorus. While this method has been proven to successfully extract phosphorus and metal compounds from freshwater sediments, it neglects to explain the biogeochemical theory behind the method. Consequently, those who have replicated the method do so in blind faith. Dithionite

obviously plays an integral role in sediment extractions, so it is important that we examine the redox kinetics of dithionite in freshwater sediments to fully understand this method

Sodium dithionite has long been used as a powerful biological reducing agent in biogeochemical research (McKenna et al., 1991).

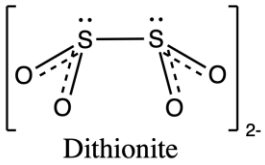

Dithionite

Figure 13. Chemical structure of the dithionite ion.

Literature values for the standard reduction potential of critical redox reactions in freshwater lake systems are shown in Table 2.

Table 2. Literature values for the standard reduction potential of critical reactions in this study (King, 2002; Harris, 1999).

Reaction	**E_0 (V)**
$CH_2O + H_2O$ (l) → CO_2 (g) + $4H^+ + 4e^-$	0.06
$Fe^{III} + e^-$ → Fe^{II}	0.771
$H_2O + e^-$ → ½H_2 (g) + OH^-	-0.828
O_2 (g) + $4H^+ + 4e^-$ → $2H_2O$	1.229
$S_2O_4^{2-}$ → SO_3^{2-}	-0.66

The dithionite ion ($S_2O_4^{2-}$) has a strong affinity for bi- and trivalent metal cations, making it an optimal choice for use in laboratory settings to mimic the reducing ability of organic carbon in freshwater lakes. In other words, dithionite acts as the inorganic surrogate for organic carbon in a laboratory setting. The use of buffered dithionite (BD) is preferred in environmental chemistry labs because organic carbon redox reactions require microbial catalysis that is often challenging to simulate *in vitro*.

Nürnberg (1988) concluded that the quantification of iron-bound phosphorus by dithionite extraction provided a more accurate estimate of internal phosphorus load in anoxic lakes when compared to other extraction reagents such as NaOH. While the Nürnberg (1988) study found that dithionite extraction correlated well with the total sediment phosphorus concentration, it neglected to correct for aluminum-bound phosphorus concentrations leading to skewed data.

In 1993, Jensen and Thamdrup published a study that drew on the Psenner and Nürnberg studies in order to modify the five-step extraction scheme for phosphorus in freshwater sediment for use in marine sediments in Denmark. The results of this study concluded that the BD-reagent is highly specific for extraction of iron-bound phosphorus (Jensen & Thamdrup, 1993).

Most of the published literature on dithionite offers a largely empirical analysis of the reducing ability of dithionite in freshwater sediments. The most extensive quantitative study of the redox potential of dithionite was that of Mayhew in 1977 in which the kinetics of the redox equilibrium established by the dithionite/(bi)sulfite system were examined. This study used dithionite as a redox reagent to react with electron carriers like flavodoxins, methyl viologen and hydrogen in the presence of catalytic hydrogenase. Previous studies have shown dithionite solutions to be strongly reducing and often assume that the dithionite/(bi)sulfite system described by equation 35 is irreversible under physiological conditions. However, several findings have indicated that there may be a redox equilibrium established by the dithionite/(bi)sulfite system at pH values ranging between pH 5 and 8 (Mayhew, 1977). The dithionite/(bi)sulfite system in question is described by the anaerobic oxidation of dithionite to (bi)sulfite:

$$S_2O_4^{2-} + 2H_2O \leftrightharpoons 2HSO_3^- + 2H^+ + 2e^- \qquad (35)$$

Mayhew (1977) concluded that the reductant in dithionite redox reagents is the dissociation product SO_2^- rather than the dithionite ion as was previously assumed. According to equation 36, the dithionite ion ($S_2O_4^{2-}$) is a dimer of SO_2^-.

$$S_2O_4^{2-} \overset{K_a}{\Leftrightarrow} 2SO_2^- \qquad (36)$$

$$K_a = \frac{[S_2O_4^{2-}]}{[SO_2^-]^2} \qquad (37)$$

SO_2^- reacts with water to form (bi)sulfite, a proton and an electron.

$$S_2O_4^{2-} \Leftrightarrow HSO_3^- + H^+ + e^- \qquad (38)$$

This means that the concentration of dithionite in solution directly (but nonlinearly) controls the concentration of SO_2^- , and thus the reducing power of the redox reagent. Of additional importance is the dependence of the midpoint redox potential of the dithionite/(bi)sulfite system (E') on the pK of (bi)sulfite at 6.9 (Mayhew, 1977):

$$HSO_3^- \overset{pK=6.9}{\Longleftrightarrow} SO_3^{2-} + H^+ \qquad (39)$$

At dithionite concentrations above 10 nM, the reductant SO_2^- is present largely in its dimeric form (Mayhew, 1977). As such, the midpoint redox potential (E_m) of dithionite solutions will become less negative (less reducing) as the concentration of dithionite is increased. In other words, the conditional redox potential of dithionite is highly dependent on the concentration of dithionite in solution.

Mayhew (1977) ultimately calculated the redox midpoint potential (E') of the dithionite/(bi)sulfite system at pH 7 to be -0.66V. The estimation for the redox potential of the dithionite/(bi)sulfite system as it relates to dithionite concentration is given by the following equation that describes the form of the redox titration curve for the dithionite/(bi)sulfite system:

$$E_h = E' + 0.0516 \log \frac{S_0}{2[S_2O_4^{2-}]} + 0.029 \log 4K_a[S_2O_4^{2-}] \qquad (40)$$

Furthermore, Mayhew predicted that the reducing ability of dithionite solution increases with increasing concentration as per the following equation:

$$E_h = E_m = E' + 0.029 \log 4K_a[S_2O_4^{2-}] \qquad (41)$$

This study provides critical insight on the reducing ability of dithionite redox reagents as a function of dithionite concentration. It additionally reinforces the notion that dithionite is a powerful reducing agent as it is a source of sulfite and bisulfite, both known reducing agents of iron. In using dithionite in our extraction protocol, we not only have a redox reagent that is sufficiently reducing but also sufficiently reactive.

In 1995, Millero et al. published a study that examined the kinetics of the rates of Fe^{III} reduction by sulfite in NaCl and seawater solutions as a function of temperature, pH, ionic strength and composition. While our study concerns strictly freshwater solutions, this study presents several important conclusions that illuminate fundamental aspects of the redox chemistry of dithionite. (1) It was found that the following reaction is first order with respect to both Fe^{III} and S^{IV}:

$$Fe(III) + S(IV) \xrightarrow{k} products \qquad (42)$$

$$\frac{d[Fe(III)]}{dt} = -k\frac{[Fe(III)]}{[S(IV)]} \qquad (43)$$

As such, the importance of Fe^{III} reduction by sulfite emerges in the context of the first-order formation of Fe^{II} in solution as a function of S^{IV} concentration. (2) The results from this paper may be applied to further examine the effect of iron speciation on the reduction rates with sulfite in natural waters. Based on their study of iron speciation in seawater as a function of pH, Millero et al. concluded that the effect of pH on the rate constant for the reduction of Fe^{III} can be described by Equation 44. At pH 7, the half-life of Fe^{II} predicted by this equation is less than one hour (Stumm, 1996; Millero et al., 1995).

$$k[Fe(III)][S(IV)] = k_0[Fe^{3+}][HSO_3^-] + k_1[FeOH^{2+}][HSO_3^-] + k_2[Fe(OH)_2^+][HSO_3^-] \quad (44)$$

The properties of dithionite have also been researched by workers in the mining community. A 2018 paper by Botelho Junior et al. investigates dithionite as a reducing agent to convert Fe^{III} to Fe^{II} in leachate from nickel mining waste. The results of this study identified dithionite as a powerful reducing agent and an optimal choice for complete conversion of Fe^{III} to Fe^{II} by reducing the potential to 590 mV at pH 0.5-2 or 240 mV at pH 2.5 (Botelho Junior et al., 2018). However, as our current study does not concern varying the potentials of our reducing reagents, the primary takeaway from the Botelho Junior study is that reducing iron with dithionite may be an optimal mechanism for the recovery of metals by an ion exchange process as Fe^{III} precipitates above pH 2 (Botelho Junior et al., 2018).

Table 3. Summary of primary conclusions from studies on the chemical behavior of dithionite as a reducing agent for Fe^{III}.

Paper	Method	Sediment type	Dithionite concentration, M	Reaction pH	Reaction temperature, °C	Reaction time, hr
Psenner & Pucsko, 1988	Empirical	Freshwater	0.1	n/a	40.00	0.5
Nürnberg, 1988	Empirical adaptation of Psenner paper	Freshwater	0.1	n/a	40	0.5
Jensen & Thamdrup, 1993	Empirical adaptation of Psenner paper	Marine	0.1	7.0	RT	1
Mayhew, 1977	Quantitative analysis of kinetics of dithionite redox equilibrium	n/a	0.1	8.5-9.0	25.00	<1
Millero et al., 1995	Quantitative analysis of Fe(III) reduction by S(IV)	Marine	1.0E-04	3.5	25.00	n/a
Botelho Junior et al., 2018	Analysis of dithionite as an iron-reducing agent	Leachate from nickel mining waste	0.1	0.5-2.0	25.00	2

11 Current study

The aims of the current study are threefold. Primarily, we will merge phosphorus concentration measurements from the empirical jar test methodology with the in-depth biogeochemical analyses of iron, aluminum and phosphorus and their interactions in freshwater lake systems. To do so, we will use data from sequential sediment extractions of samples from Great Pond and China Lake, and introduce an analysis of the reductive dissolution of phosphorus as a function of Al:Fe. Additionally, we will provide critical insight into the chemical behavior of dithionite as a reducing agent by determining the optimal reaction time for the dithionite extraction step. We will relate our discussion of the dithionite reaction time to the chemical foundations drawn from literature presented the above sections. Finally, as we hypothesize that our conclusions from our adapted jar test procedure will be consistent with our geochemical extraction data, we aim to make a recommendation for future studies that underscores the importance of including iron and aluminum data in water quality management schemes. Since most researchers do not focus on iron and aluminum concentrations in their sediments, they have no context in which to compare internal phosphorus cycling across different lakes. Thus, we ultimately propose that future alum dose engineering studies consider iron and aluminum data in tandem with their phosphorus data in order to achieve a comprehensive understanding of the biogeochemistry of phosphorus cycling in freshwater lakes.

MATERIALS AND METHODS

1 Sediment sampling

1.1 Site description

The Belgrade Lakes region and surrounding watersheds (Figure 14) were selected for sediment analysis of phosphorus cycling based on historical patterns of seasonal anoxia and algal blooms. Among the identified lakes, East Pond, North Pond, Great Pond, Salmon Pond and China Lake (not in the Belgrades, but central to this study) were eutrophic or mesotrophic (high phosphorus) while the other three (Long Pond, Messalonskee Lake and McGrath Pond) were oligotrophic or mesotrophic (low phosphorus) (Ferwerda et al., 1997). All 8 lakes share similar hydrologic characteristics (Table 4). Sediment fractionation data presented in this study results from extraction analyses of East Pond, Great Pond and China Lake, however water quality levels of all 8 lakes have been monitored consistently throughout the course of this study.

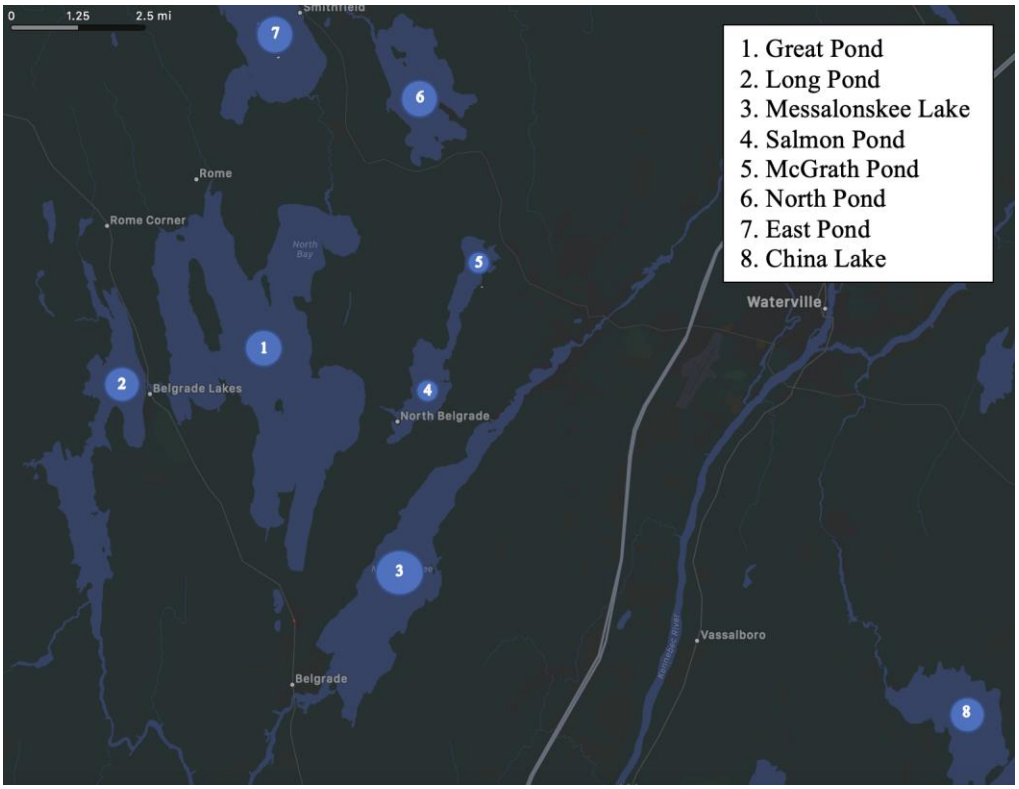

Figure 14. Map of Maine lakes involved in this study.

Table 4. Hydrologic properties of 8 Maine Lakes involved in this study. Data from Lake Stewards of Maine.

Lake	Mean depth (m)	Max depth (m)	Perimeter (km)	Surface area (ha)
Great	6.4	21	74	3453
Long	11	32	50	1035
Messalonksee	10	34	48	1494
Salmon	7	17	13	281
McGrath	5	8	11	189
North	4	6	15	1024*
East	5	8	22	695
China	9	26	49	1594

* combined area of North Pond and Little North Pond

1.2 Sampling protocol

Lake bottom sediment samples were collected using a Standard Ekman Grab Kit from frozen (if possible) lakes. Sediment samples cores were taken between 0 and 10 cm below the sediment-water interface. In the lab, samples were composited by depth, transferred to airtight freezer bags and stored at -80ºC for preservation. To prepare samples for extraction, they were removed from the freezer, allowed to thaw overnight and set to dry thoroughly under a laminar flow hood for 24-72 hours.

1.3 Sediment moisture and organic matter content

The moisture content of each sample was determined by Thermogravimetric Analysis (TGA). TGA allowed us to monitor the mass of each sediment sample as a function of temperature in order to quantify loss of water and organic material upon heating. The King Lab TGA method involved heating the samples to 150ºC, measuring the loss of water, and then heating to 500ºC, and measuring the loss of organic carbon. Samples were also oxidized with H_2O_2 and similarly analyzed with TGA in order to determine their inorganic carbon fraction.

2 Experimental alum dosing

Samples were treated with an alum solution prepared by adding 1 mL USALCO® Acid Alum Aluminum Sulfate Solution and 0.5 mL USALCO® 38 Sodium Aluminate Solution to 30 mL 18.0 MΩ purified reagent water. 6 different alum doses were delivered to sediments according to Table 5.

Table 5. Alum dose preparation.

Alum dose, g/m^2 sed	Vol alum soln, µL
0	0
4	100
7	200
15	400
29	800
58	1600

3 Sediment extraction

The King Lab at Colby College developed a sediment fractionation method based on that published by Psenner and Pucsko (1988) to extract phosphorus and metal compounds from freshwater sediments. All reagents were made using 18.0 MΩ purified reagent water. 1 gram of sediment from each sample was used for extraction. The extraction procedure was as follows (see Table 6 for pH and redox potential parameters): (1) 1 M NH_4Cl for 2 hours at RT to extract weakly bound Fe, Al and P; (2) 0.11 M Na_2SO_4-buffered $NaHCO_3$ for 2 hours at RT to extract Fe and P released under anoxic conditions; (3) 0.1 M NaOH for 24 hours at RT to extract any remaining Al in sediment. The samples were placed on an automatic spinner for the entirety of the reaction period. Samples were centrifuged at 4000xg for 15 min and the supernatant was decanted. 0.5 mL of each supernatant was transferred into 10 mL of 3% HNO_3 to prepare samples for analysis of Fe, Al and P using an Inductively Coupled Plasma – Emission Spectrometer (ICP-ES). (See Appendix C for a more detailed protocol.)

4 Measuring pH and redox potential

The redox potential of each reagent was measured in mV before and after each reaction using a redox probe and the measurements were standardized with a commercial ZoBell solution. The pH of each reagent before extraction was measured using a Fisherbrand probe. Table 6 shows the desired redox potential and pH ranges of the first two extraction steps. The redox and pH parameters of the NaOH extraction step are not significant to our data as the point of this extraction is to dissolve any remaining aluminum from the sediment samples.

Table 6. Optimal pH and redox potential range for ammonium chloride and sodium dithionite. extraction reagents.

	pH	redox potential, mV
ammonium chloride, stock	7.5 to 8.5	85 to 145
dithionite, stock	6.5 to 7.5	-500 to -600

5 Dithionite stability

Sodium dithionite is a highly reactive compound, and the literature is inconsistent on the parameters of sediment extraction using dithionite as the reductive step (Table 3). Thus, this work aims to characterize the optimal extraction conditions (concentration, temperature, time) for the dithionite extraction step. The primary issue when working with sodium dithionite solution is shelf life. In our lab, we pre-made our bicarbonate buffer solution and added powdered sodium dithionite to the buffer immediately before use. Based on previous studies, we used 0.1 M dithionite for all experiments. Similarly, we concluded that performing the dithionite extraction at RT would provide optimal data.

In order to determine the ideal reaction time for sediment extraction with dithionite, we performed a series of experiments, varying the reaction times from 2 to 48 hours. 1 gram of sediment was extracted first with ammonium chloride and then with dithionite. Supernatant

samples at roughly two-hour intervals throughout the course of the dithionite extraction were taken, and the concentration of reductive phosphorus released was analyzed using the ICP-ES.

6 Data analysis

Raw data from the ICP-ES for concentrations of Fe, Al and P were measured in parts per billion (ppb) and converted to g/m^2 using molar mass, stoichiometry, density, etc. as detailed in Appendix C.

RESULTS AND DISCUSSION

1 TGA analysis of air-dried sediment samples

We performed TGA on air-dried sediment samples in order to characterize the percent organic carbon in each sample. As organic carbon plays a role in the reductive capability of lake-bottom sediments (more DOC means more reducing ability; Figure 7), it is important to characterize the percent organic carbon by mass of the sediments. Figure 15 shows the percent organic carbon of sediment samples from China Lake.

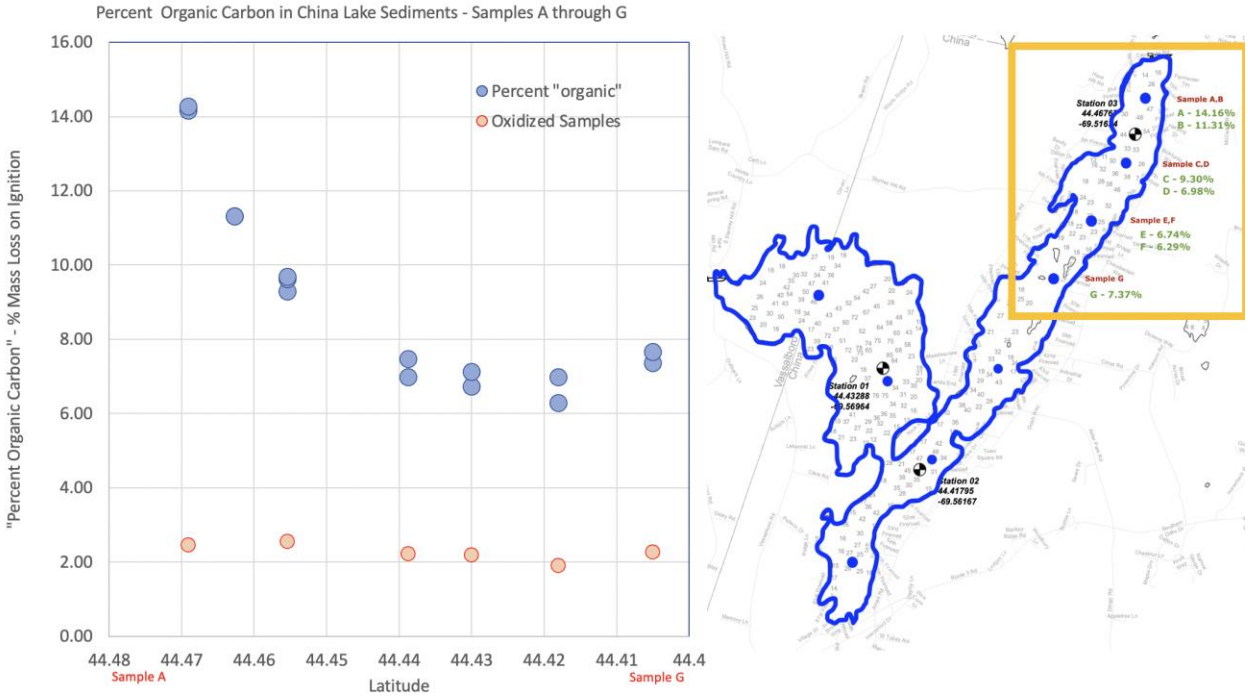

Figure 15. Percent organic carbon of sediments from several China Lake sampling locations.

The blue plot on the left side of Figure 15 shows a clear decrease in mass lost on ignition as we move from sample A (the north end of the lake) to sample G (further south in the lake). This means that sediments from the northern end of China Lake have more organic carbon than sediments more toward the middle. As we see the most intense instances of algal blooming on the north end of China Lake, this data makes sense as increasing organic carbon represents decreasing water quality. Ultimately, the TGA analysis of our sediment samples plays an

important role in our understanding of the relative reducing capabilities of the sediments, separate from the reducing ability of dithionite. Although, reduction via the organic carbon fraction of the sediments is nearly negligible when using one-gram samples as we do in this study.

The "oxidized samples" plot represents samples oxidized with H_2O_2. This data suggests that all of our sediments have a consistent 2% inorganic carbon fraction (likely $CaCO_3$ (s)). This data is meant as a quality check to make sure our percent organic carbon data does not reflect loss on ignition of other inorganic molecules.

2 Determining optimal reaction time for dithionite extraction

In order to determine the optimal reaction time for the dithionite extraction step, we performed a time trial experiment in which we varied the reaction time from 2 hours to 48 hours. Figure 16 demonstrates the reductive phosphorus release as a function of reaction time with 0.1 M dithionite at RT. Similarly, Figure 17 demonstrates the redox potential of the same dithionite extraction solution as a function of time.

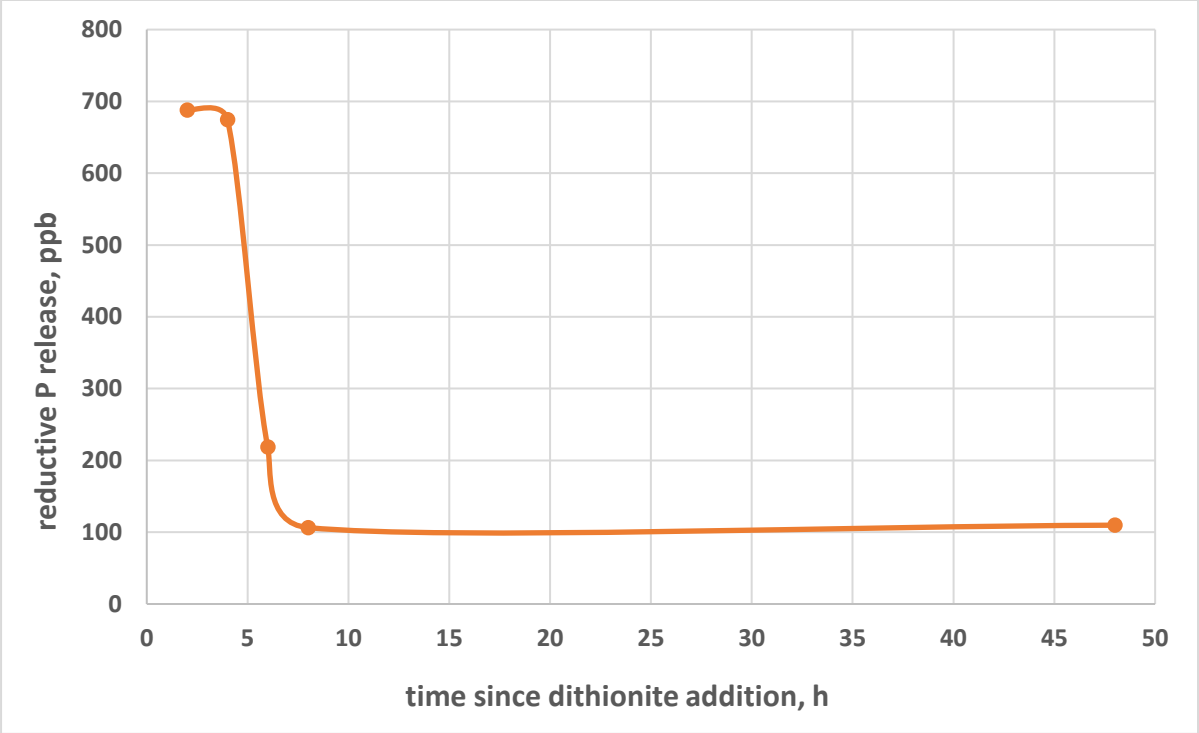

Figure 16. Reductive phosphorus release as a function of reaction time.

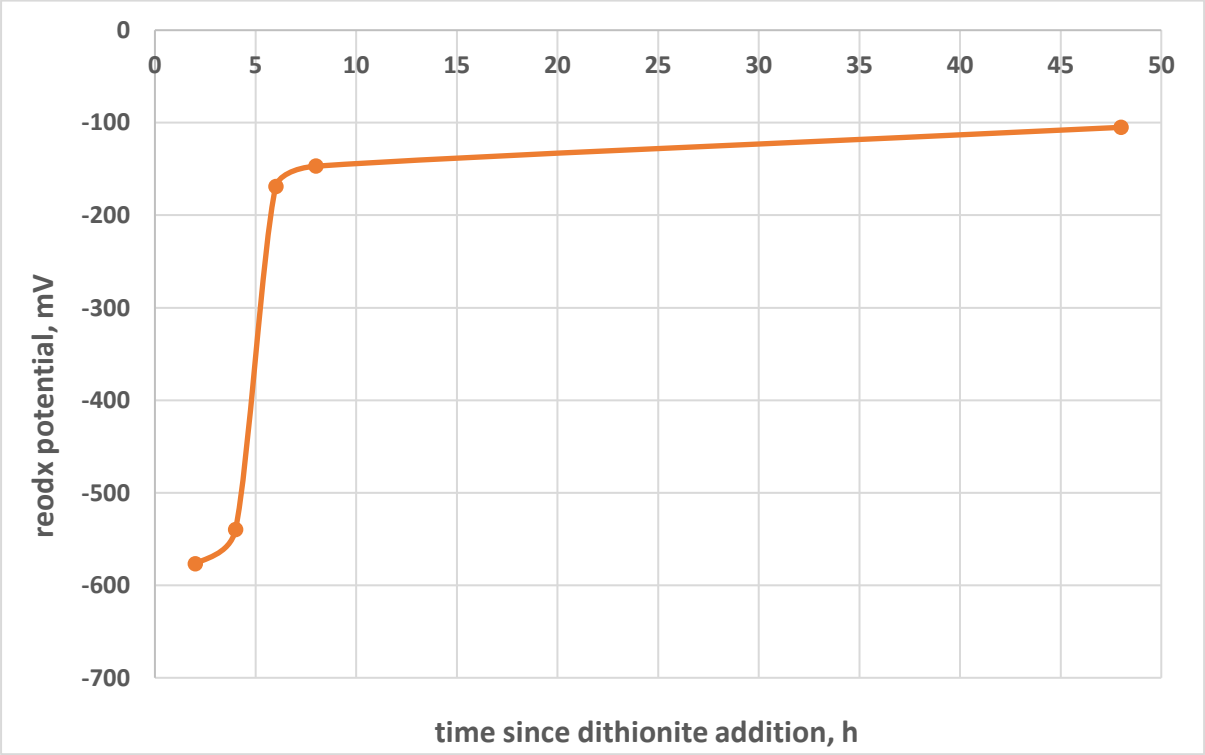

Figure 17. Redox potential of dithionite extraction reagent as a function of reaction time.

From the data presented in Figures 16 and 17, we see a dramatic drop in both reductive phosphorus release and redox potential around hour 3 or 4. Since the dithionite reagent is meant to mimic the reducing conditions of the lake, as the magnitude of the redox potential decreases (aka becomes less negative), the dithionite reagent becomes decreasingly reductive and increasingly ineffective. Thus, we recommend a two-hour reaction time in the dithionite extraction step so that the reagent is at its peak redox potential for the entirety of the reaction. These findings are consistent with our greater understanding of dithionite. We know that dithionite is highly volatile as it reacts freely with oxygen in the air (King, 2002). Since this experiment required an increase in exposure to air, it is likely that the decrease in redox potential (Figure 17) is more profound than it would be in a typical extraction procedure. Reproducing this experiment is a critical step in furthering our understanding of the volatility of dithionite however this data does provide promising foundational insight.

3 Sequential extractions of sediments from Great Pond and China Lake

Sequential sediment extractions raw data

We performed a series of sequential sediment extractions with intentionally added aluminum on samples from two Maine Lakes (Great Pond and China Lake) to quantify reductive phosphorus release as a function of added aluminum concentration. Appendix D shows the raw extraction data from these experiments. Total extractable phosphorus in the absence of added aluminum ranged from approximately 2 to 22 g/m^2 across both lakes. The largest percentage of extractable phosphorus in all samples was in the NaOH extraction step, however, in the majority of the samples, the dithionite extraction step yielded a significant amount of extractable phosphorus when compared to the ammonium chloride extraction step. This once again makes sense in terms of the Pourbaix diagrams (Figure 9) as we understand that the dithionite extraction reduces Fe^{III}

species to the Fe^{II} species that we know to release phosphorus into the water column. Total extractable iron ranged from approximately 3 to 135 g/m^2 across both lakes. The major percentage of extractable iron was in the dithionite fraction. Finally, total extractable aluminum (excluding intentionally added aluminum) ranged from approximately 7 to 27 g/m^2 across both lakes. The majority of all extractable aluminum was extracted in the NaOH extraction step.

Plotting reductive phosphorus release as a function of added aluminum and Al:Fe

Figures 18 and 19 show the reductive phosphorus release as a function of aluminum dose and Al:Fe for each of the two lakes.

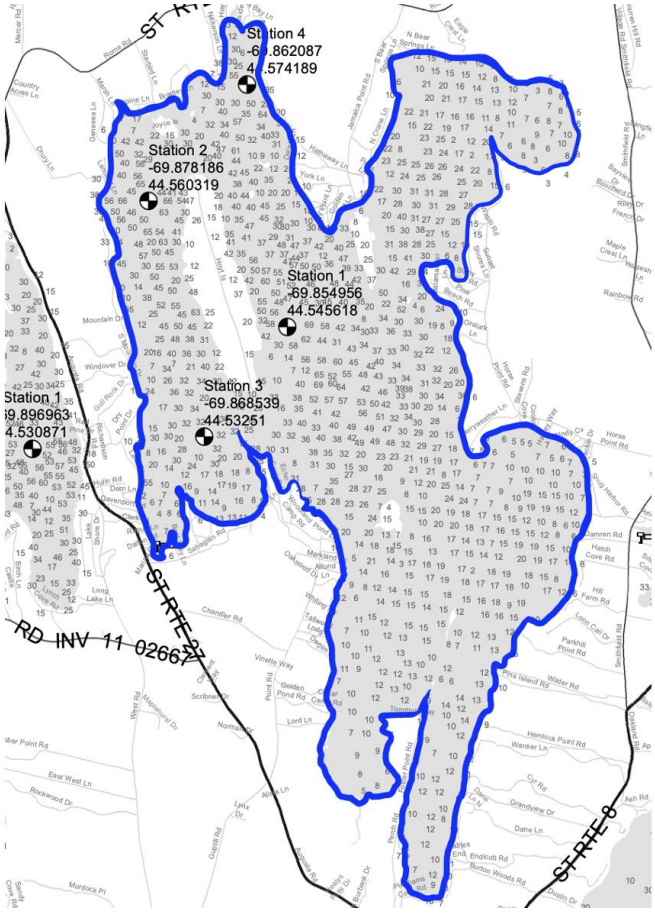

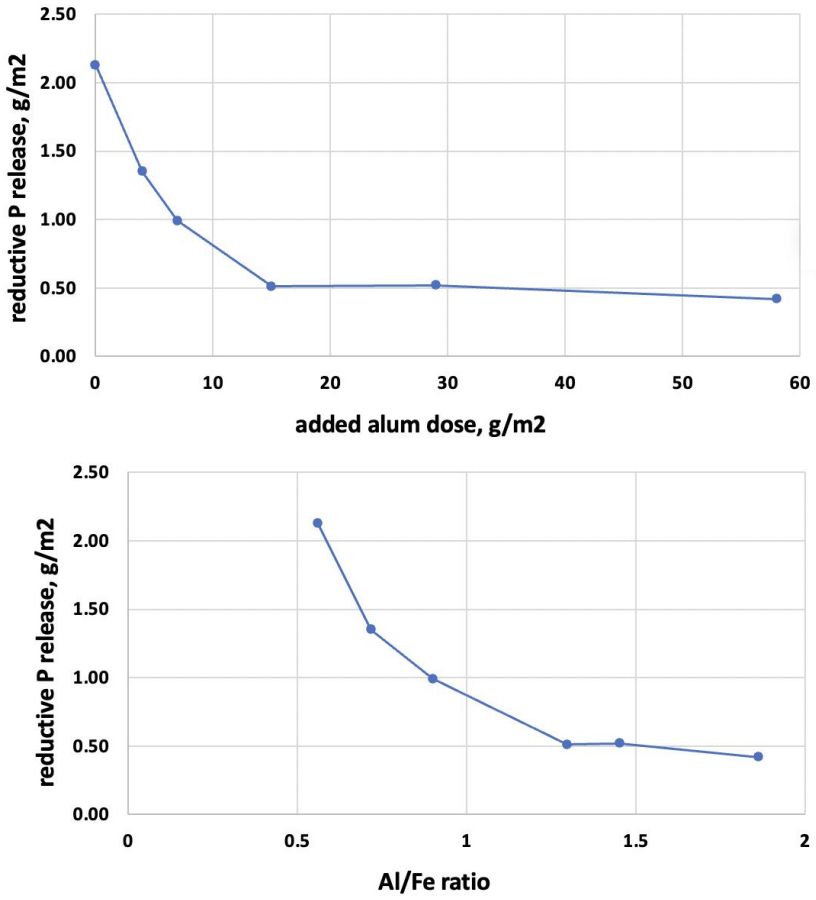

Figure 18. Sequential sediment extraction data from Great Pond.

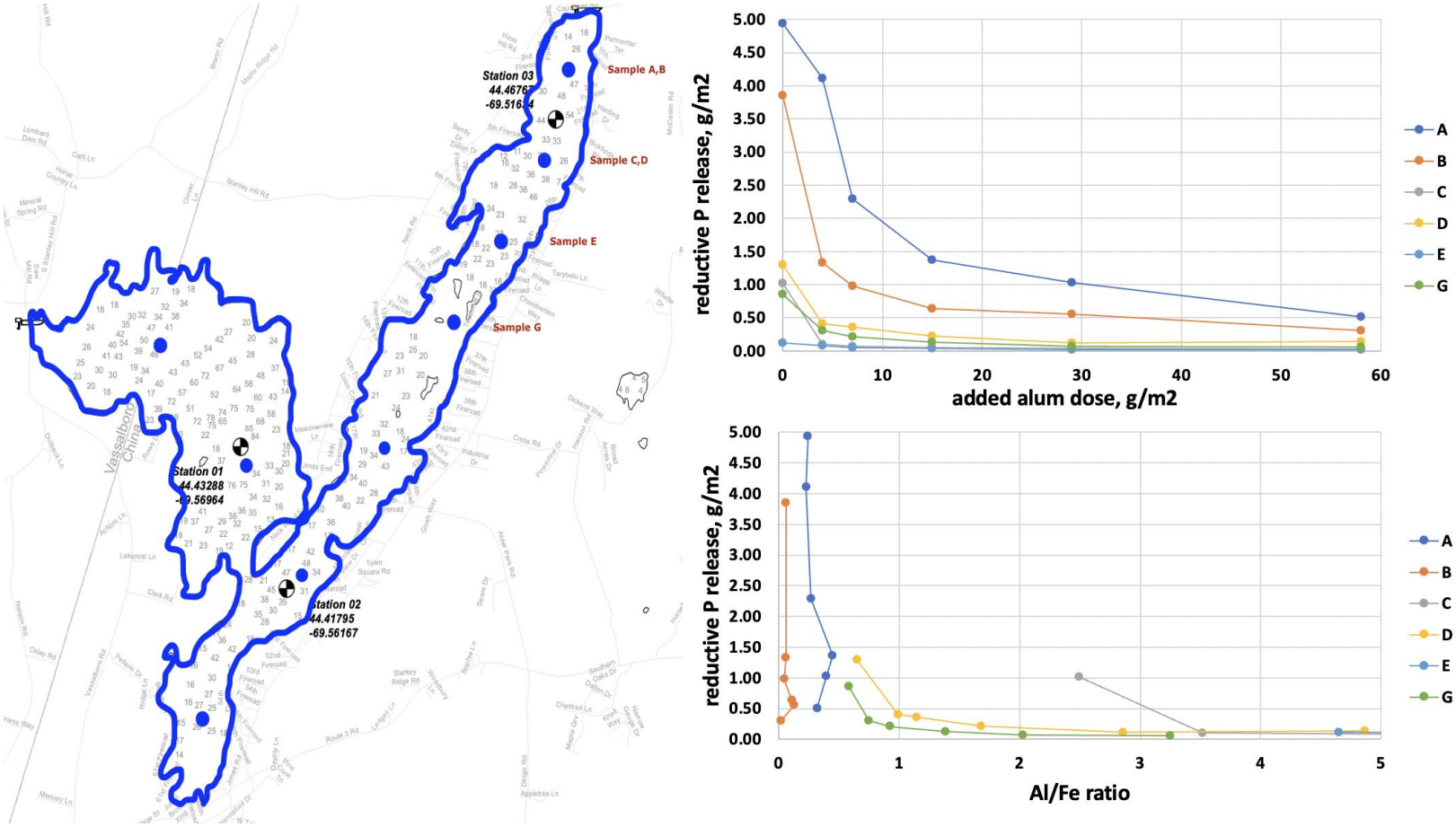

Figure 19. Sequential sediment extraction data from China Lake.

Understanding our data in terms of Al:Fe

Conventional aluminum dose curves such as the top plots in Figures 12, 18 and 19 are typically used for empirical aluminum treatment engineering. These curves simply show that as intentionally added aluminum increases, phosphorus release from sediments decreases. Thus, the proposed aluminum dose is the aluminum concentration at which the reductive phosphorus release begins to level off. Incorporating these dose curves into our analysis of lake systems geochemistry is important but does not tell the whole story. In order to develop reasonable models for the biogeochemistry of phosphorus cycling, we must also include chemical analyses of the ambient concentrations of iron and aluminum in the lake bottom sediments.

Phosphorus is most often found in freshwater lakes complexed with Fe^{III} and Al^{III} solids. As such, the literature has demonstrated that the ratios between phosphorus and iron or aluminum, in addition to Al:Fe, can provide critical insight into the trophic status of a lake (Amirbahman et al., 2003; Kopáček et al., 2001). Therefore, we included the plots of reductive phosphorus release as a function of Al:Fe in Figures 12, 18 and 19. These plots have the same characteristic curve shape as the alum dose plots. However, they allow us to condense a range of samples from a single lake so that we can visualize Al:Fe throughout the lake.

The relationship between the reductive phosphorus release and Al:Fe provides insight into lake-bottom sediment chemistry. Historically, iron and aluminum concentrations in the sediments are critical yet often neglected aspects of P flux analysis. The literature has demonstrated that naturally occurring lakes that do not suffer from algal blooming have less phosphorus so that ambient aluminum levels can successfully mitigate P flux into the water column (Kopáček et al., 2005). Conversely, lakes that do bloom likely have too much phosphorus so that there is no natural ability (naturally occurring aluminum) to combat this. We

see this phenomenon played out in our data; it is most apparent in our China Lake extraction data. From looking at Figure 19, it is immediately obvious that samples with a higher Al:Fe have less phosphorus release than samples with a lower Al:Fe. Furthermore, samples from the north end of the lake (particularly samples A and B) have much higher levels of reductive phosphorus release than other samples (Figure 19). From our ICP data, we know that samples A and B also have relatively high iron levels compared to the other samples. Table 7 shows average Al:Fe at each sampling location.

Table 7. Average Al:Fe at each sampling location on China Lake.

Sample	Average [Al], g/m2	Average [Fe], g/m2	Average Al:Fe
A	28.35	107.37	**0.264**
B	4.00	96.66	**0.041**
C	9.17	1.29	**7.138**
D	60.61	60.89	**0.995**
E	40.33	6.82	**5.911**
G	43.84	61.10	**0.718**

Note that the northern most samples (sample A and sample B) have the lowest Al:Fe and the highest iron concentrations. This makes sense with the extraction curves as we would expect high iron levels to translate to high phosphorus release under reducing conditions. Zooming out, this data makes perfect sense with the overall biochemistry of the lake as the algal blooms at the north end of China Lake are the worst. There is a marsh just to the north of China Lake and we hypothesize that this marsh is responsible for the phosphorus and iron trends we are seeing in the lake. The marsh is expected to be reductive, and as it goes anoxic it releases iron that gets carried into the north end of China Lake and subsequently precipitates. As a result, ambient Al:Fe in the north end of China Lake is very low and cannot mitigate reductive phosphorus release as well as other areas of the lake with higher Al:Fe (Figure 19).

Investigating the chemical rational underlying the Al:Fe plots

China Lake is a fascinating lake to be studying currently because it perfectly demonstrates the importance of Al:Fe in terms of understanding internal P flux. Engineers would likely look at this lake and dump more aluminum that necessary into it. However, it would be much more practical to develop a model that allows us to easily characterize phosphorus release as a function of Al:Fe so that we can tailor our aluminum treatment in a way that minimizes cost and maximizes impact. That is, rather that uniformly dumping a certain amount of aluminum across the whole lake, we could instead base our treatment recommendation based on the natural Al:Fe gradient throughout the lake. Areas with naturally high aluminum and low iron would need less added aluminum than areas with naturally low aluminum and high iron.

Ultimately, this idea brought us to trying to understand the chemical rational behind the Al:Fe plots. We want to know why Al:Fe is such a strong indicator of reductive phosphorus release in freshwater lake systems. While these plots confirm what we already empirically know – that more aluminum translates to less reductive dissolution of phosphorus 00 they do not tell us why. The logical next step in this investigation is thus to look into the nature of chemical adsorption patterns of phosphorus in freshwater lake systems. We want to know if our observations from Figures 12, 18 and 19 make chemical sense based on what we know about phosphorus adsorption to iron and aluminum.

CONCLUSION

This thesis effectively characterizes the interface between the empirical jar test methodology and in-depth biogeochemical analyses of iron, aluminum and phosphorus concentrations in freshwater lake systems. As the extraction methods were altered between the East Pond experiment and the Great Pond and China Lake experiment, we unfortunately cannot make assumptions based on comparisons of total extractable iron, aluminum and phosphorus levels between these three lakes. However, we have successfully defined the experimental methodology for sequential sediment extraction and analysis that will guide future research to easily and accurately compare the iron, aluminum and phosphorus levels of many lakes.

The primary conclusion of this thesis is that data from our adapted jar test procedure is completely consistent with our biogeochemical analysis of our extraction data. We also conclude that characterizing the chemical behavior of dithionite is critical for a full understanding of this research, and that despite a high degree of uncertainty in the literature, the optimal reaction time for the dithionite extraction step in undoubtedly 2 hours. Finally, we conclude that it is critical that freshwater lake scientists continue to consider both sides of the story; since most researchers do not focus on iron and aluminum concentrations in their sediments, they have no context in which to compare lakes. Ultimately, we propose that proper analysis of iron and aluminum levels in lake-bottom sediment samples is an integral aspect of this field of work. Future aluminum treatment engineering projects must include iron and aluminum data in all of their measurements in order to achieve a comprehensive understanding of the biogeochemistry of phosphorus cycling in freshwater lakes.

Future directions

An important experiment to expand our understanding of the chemical nature of phosphorus adsorption to iron and aluminum involves an investigation of the Fe-P and Al-P binding kinetics. We propose that future studies begin to look at phosphorus release at regular intervals starting immediately after dithionite introduction up to 2 hours post-addition. Figure 20 shows a schematic for what we expect is happening with P flux under reducing conditions.

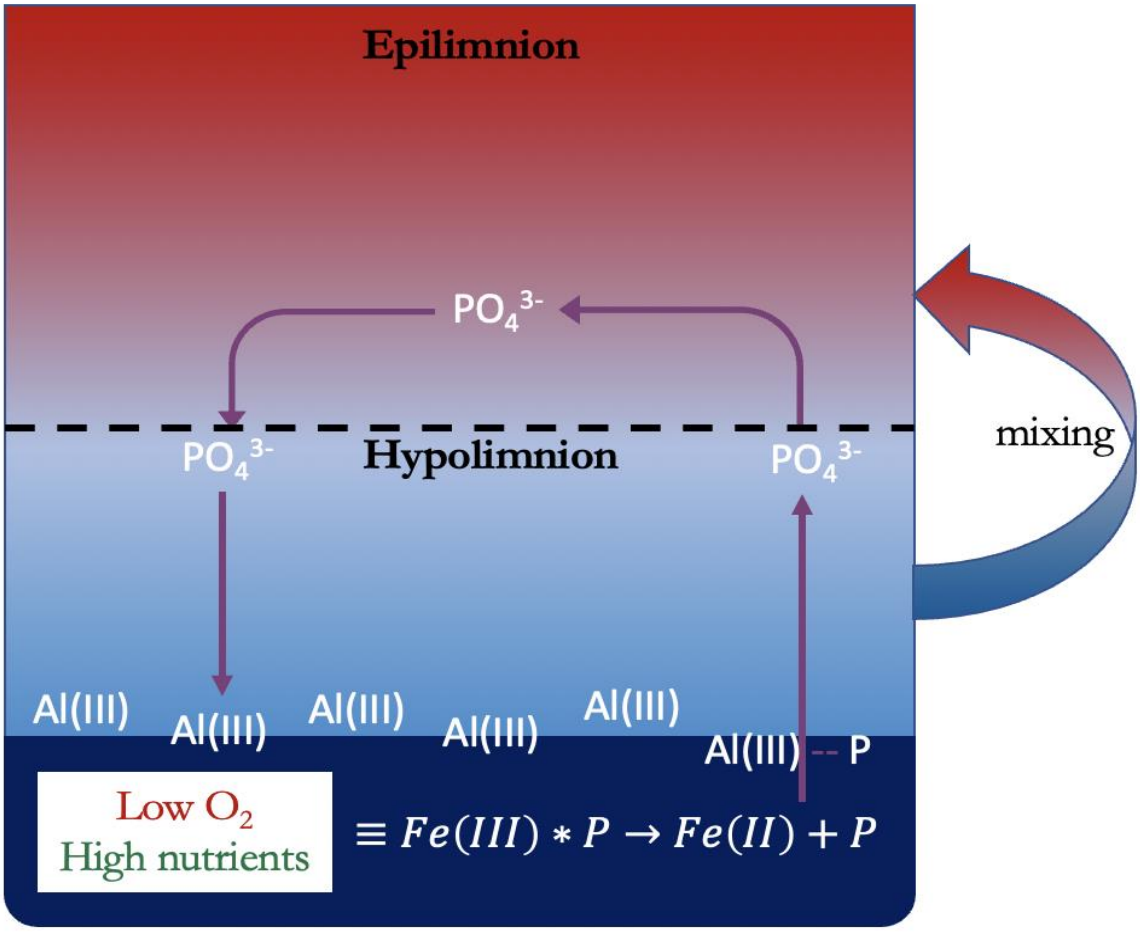

Figure 20. Schematic for proposed trajectory of reductive phosphorus release from lake bottom sediments. Upon reductive dissolution, phosphorus is released into the water column as phosphate. We hypothesize that a small fraction of dissolved phosphorus binds with adjacent Al^{III} in the sediments while the majority binds to Al^{III} after floating down through the water column.

(I) represents phosphorus dissociation from iron upon reduction of Fe^{III} to Fe^{II}; (II) represents the max phosphorus dissociation from the reduced iron; and (III) represents the aluminum binding to dissolved phosphorus. We hypothesize that the reduction of iron and dissolution of iron-bound phosphorus is fast compared to Al-P complexation. This assumption is based on our chemical extraction data; in our jar test experiments, there is an abundance of aluminum relative to phosphorus. Thus, we would expect that all phosphorus released upon the reduction of iron would immediately be trapped by aluminum, however, based on our ICP extraction analysis, this does not seem to be the case. As such, we have identified an area of incredible uncertainty in our understanding of Fe-P and Al-P binding kinetics in lake bottom sediments. Revealing the precise kinetics of phosphorus adsorption to iron and aluminum has the potential to dramatically change the traditional methods of aluminum treatments to mitigate internal P flux. It will also open the door for future researchers to find new ways to streamline conventional water quality management strategies.

ACKNOWLEDGEMENTS

First and foremost, I would like to thank my research mentor, Professor Whitney King, not only for advising my Honors Thesis, but for all of the academic, professional and personal support he has provided me over the past four years. To Whitney, thank you for all of the time you spent with me, teaching me how to conduct research, to learn from my mistakes and to think analytically.

I would also like to thank Professor Denise Bruesewitz and Doctor Benjamin Twining for acting as my second readers. Their feedback has been an invaluable resource for my thesis. Similarly, I would like to thank the Seven Lakes Alliance in Belgrade, ME for sponsoring my research over the past four years.

Additionally, I would like to thank all of the King Lab members, both past and present. Joining the King Lab as a freshman was both overwhelming and exciting, and many of the upperclassmen members made my transition into research effortless. I would especially like to thank Emily Visco ’20, Sarah Vaughan ’20, Guillermo Pico Oms ‘19 and Lilly Naimie ’19.

Finally, I would like to thank all of the professors and students in the Colby College Chemistry Department. I am forever grateful for the unwavering support, dedication and respect that I received from each and every one of you. My time at Colby has been made infinitely better by the long nights in Keyes, engaging conversations and truly remarkable relationships I have formed with so many of you.

Thank you, Colby, for grounding me for the past four years. You will always have a very special place in my heart, and I am so excited to move on knowing I will always be a part of the Colby community.

REFERENCES

1. Amirbahman A, Pearce AR, Bouchard R, Norton SA, Kahl SK. Relationship between hypolimnetic phosphorus and iron release from eleven lakes in Maine, USA. *Biogeochemistry*. 2003;65:369–86.
2. Botelho Junior A, Jiménez Correrea M, Espinosa DCR, Tenório JAS. Study of the reduction process of iron in leachate from nickel mining waste. *Braz. J. Chem. Eng*. 2018;35(04):1241-1248.
3. Lake B, Coolidge K, Norton S, Amirbahman A. Factors contributing to the internal loading of phosphorus from anoxic sediments in six Maine, USA, lakes. *Sci. Total Environ.* 2007; 373:534-541.
4. Ferwerda JA, LaFlamme KJ, Kalloch NR Jr., Rourke RV. The Soils of Maine. *Maine Agricultural and Forest Experiment Station.* 1997; 402:5-20.
5. Gächter R, Meyer J. The role of microorganisms in mobilization and fixation of phosphorus in sediments. *Hydrobiology*. 1993;253:103–21.
6. Harris DC (1999). *Quantitative Chemical Analysis* (Eighth ed.). New York, NY: W. H. Freeman and Company.
7. Hem JD & Cropper WH. Chemistry of iron in natural water: Survey of ferrous-ferric chemical equilibria and redox potential. *Geological Survey Water-Supply Paper*. 1962.
8. Jansson M. Anaerobic dissolution of iron-phosphorus complexes in sediment due to the activity of nitrate-reducing bacteria. *Microb. Ecol.* 1987;14:81-89.
9. Jensen HS, Thamdrup, B. Iron-bound phosphorus in marine sediments as measured by bicarbonate-dithionite extraction. *Hydrobiologia*. 1993;253:47-59.
10. King DW. A General Approach for Calculating Speciation and Poising W Capacity of Redox Systems with Multiple Oxidation States: Application to Redox Titrations and the Generation of pE–pH Diagrams. *J. Chem. Ed.* 2002; 79(9): 1135-1140.
11. King, Whitney: personal communication.
12. Kopáček J, Hejzlar J, Borovec J, Porcal P, Kotorová I. Natural inactivation of phosphorus by aluminum in atmospherically acidified water bodies. *Limnol. Oceanogr.* 2000;45:212–25.
13. Kopáček J, Ulrich K, Hejzlar J, Borovec J, Stuchlik E. Phosphorus inactivation by aluminum in the water column and sediments: lowering of in-lake phosphorus availability in an acidified watershed-lake system. *Wat. Res.* 2001;35:3783–90.
14. Kopácek, J, Borovec, J, et al. Aluminum control of phosphorus sorption by lake sediments. *Environ Sci Technol.* 2005;39:8784-8789.
15. Madore D. Maine's lakes could experience increased algae blooms this summer. *Maine Department of Environmental Protection.* 2020.
16. Mayhew SG. The Redox Potential of Dithionite and SO_2^- from Equilibrium Reaction with Flavodoxins, Methyl Viologen and Hydrogen plus Hydrogenase. *Eur. J. Biochem.* 1978;85:535-547.

17. McKenna CE, Gutheil WG, Song W. A method for preparing analytically pure sodium dithionite. Dithionite quality and observed nitrogenase-specific activities. *Biochim Biophys Acta.* 1991;1075(1):109-117.
18. Millero FJ, Gonzalez-Davila M, Santana-Casiano JM. Reduction of Fe(III) with sulfite in natural waters. *J. Geophys. Res.* 1995;100(D4):7235-7244.
19. Nesbeda RH. Sedimentological and geochemical characterization of East Pond, Belgrade Lakes
20. Watershed, Central Maine. *Colby College Honors Thesis.* 2004.
21. Norton SA, Coolidge K, Amirbahman A, et al. Speciation of Al, Fe, and P in recent sediment from three lakes in maine, USA. *Science of the Total Environment.* 2008;404(2-3):276-283.
22. Nürnberg GK. Prediction of phosphorus release rates from total and reductant-soluble phosphorus in anoxic-lake sediment. *Can. J. Fish. Aquat. Sci.* 1988;45:453-462.
23. Phosphorus Control Action Plan: Echo Lake – Presque Isle, Aroostook County, Maine. (2007). *Echo Lake PCAP – TMDL Report, Maine DEPLW – 0812.*
24. Porcal P, Amirbahman A, Kopáček J, Norton SA. Experimental photochemical release of organically bound aluminum and iron in three streams in Maine, USA. *Environ. Monit. Assess.* 2010;171:71-81.
25. Psenner R, Pucsko R. Phosphorus fractionation: advantages and limits of the method for the study of sediment P origins and interactions. *Arch. Hydrobiol. Beih.* 1988;30:43–59.
26. Ptacnik R, Anderson T, Tamminen T. Performance of the Redfield Ratio and a Family of Nutrient Limitation Indicators as Threshold for Phytoplankton N vs. P Limitation. 2010;13:1201-1214.
27. Schindler DW. Evolution of phosphorus limitation in lakes. *Science* 1977;195:260–2.
28. Smith RM, Martell AE (1989). *Critical stability constants*. New York, NY: Plenum Press.
29. Song K, Adams CJ, Burgin AJ. Relative importance of external and internal phosphorus loadings on affecting lake water quality in agricultural landscapes. *Ecological Engineering.* 2017;108(B):482-488.
30. Stumm W, Morgan JJ (1996). *Aquatic chemistry* (Third ed.). New York, NY: Wiley.
31. The Economics of Lakes - Dollars and $ense. (n.d.). Retrieved January 27, 2021, from https://www.maine.gov/dep/water/lakes/research.html#f4
32. Wagner, Ken: personal communication.

APPENDIX A: Dissociation constants for PO_4^{3-}, Fe, and Al species.

	K	pK
H_3PO_4 D $H_2PO_4^-$ + H^+	6.9 x 10^{-3}	2.16
$H_2PO_4^-$ D HPO_4^{2-} + H^+	6.2 x 10^{-8}	7.21
HPO_4^{2-} D PO_4^{3-} + H^+	4.8 x 10^{-13}	12.32
$FeOH_2^+$ D FeOH + H^+	--	6.00
FeOH D FeO^- + H^+	--	7.70
$AlOH_2^+$ D AlOH + H^+	--	7.29
AlOH D AlO^- + H^+	--	8.93

APPENDIX B: Sediment analysis methods

I. EQUIPMENT, INSTRUMENTATION

A. Laminar flow hood
B. Mechanical spinner
C. Centrifuge
D. ICP-ES instrument

II. EXTRACTION SOLUTION PREPARATION

A. *Aluminum Dosing*

(i) USALCO 38: Sodium Aluminate solution
Specific gravity = 1.46 - 1.49
pH = 14
% Al203 = 19.5 - 20.5

(ii) USALCO Acid Alum: Aluminum Sulfate solution
Specific gravity = 1.28 - 1.30
pH = 0.2 - 1.0
% Al203 = 5.8 - 6.2

(iii) Aluminum dosing
Add 2 ml aluminum sulfate (acid) and 1 ml sodium aluminate (base) to 30 ml deionized water in a beaker with a stir bar to make 2:1 alum stock solution. Continue stirring so as not to allow flock to settle out. Use Table 1 to prepare alum dosed samples. *Remake 2:1 alum stock solution at the start of each day.*

Table 1. Alum flock solution preparation.

Approx. alum dose (mg Al/g)	Vol 2:1 stock (µl)
0	0
4	100
7	200
15	400
29	800
58	1600

B. *Ammonium Chloride solution.*
Partially fill a 1L beaker with reagent water. Add 67 mL of concentrated ammonium hydroxide and 82 mL of concentrated hydrochloric acid. Fill to the 1L mark with more water. Adjust pH to 8.5 with more hydrochloric acid. *This solution is stable for 1 year.*

C. *Buffered Dithionite solution*
Partially fill a 1L beaker with reagent water. Add 9.2 grams of sodium bicarbonate and adjust pH to 7.0-7.5 with concentrated sodium hydroxide. Fill to 1L. *This solution is*

stable for 1 year. Before each dithionite extraction, add 4.8 g sodium hydrosulfite (sodium dithionite) to 250 mL of the buffer solution. *This solution is stable for one week.*

D. *Sodium Hydroxide solution*
Partially fill a 1L beaker with reagent water. Add 40.00 grams of sodium hydroxide pellets. Add more water to bring the solution up to the 1L line. *This is a 1M NaOH solution.* Dilute ten times to create the 0.1M solution that will be used in the sediment extractions. *This solution is stable for one year.*

III. PROCEDURE

A. Extraction solutions

1. Sediment samples stored in -80ºC *(we currently do not have -80 freezers so samples will in King lab freezer)* should be removed approximately 12 hours before use to allow proper defrosting.
2. Allow samples to dry thoroughly (1-2 days) in weigh boats under a laminar flow hood in clean room.
3. Add approximately 1 g of dried sediment to 6, 50 mL conical tubes.
4. Ammonium chloride fraction
   a. Add 5-10 mL of Ammonium chloride solution directly to dried sediment in each tube.
   b. Measure redox potential (should be close to that of ammonium chloride).
   c. Add 2:1 alum stock solution to each tube according to Table 1.
   d. Add additional ammonium chloride to the 30 mL mark on each tube.
   e. Record pH of each sample (should be consistent and around 7).
   f. Allow tubes to spin at 30 RPM for 2 hours using a mechanical spinner.
   g. Centrifuge tubes at 4000 RPM for 15 minutes.
   h. Pour off each supernatant into a clean, labelled Falcon tube.
5. Buffered dithionite fraction
   a. Add 30 mL of the buffered dithionite solution to the 6 original tubes.
   b. Measure redox potential (should be close to that of BD).
   c. Allow tubes to spin for 2 hours at room temperature.
   d. Spin, centrifuge, and pour off supernatant exactly as done in the previous step.
6. Sodium hydroxide fraction
   a. Add 30 mL of the 0.1M NaOH solution to the 6 original tubes.
   b. Allow tubes to spin for 24 hours at room temperature
   c. Spin, centrifuge, and pour off supernatant exactly as done in the previous step.

B. ICP sample preparation

- To prepare ICP sediment samples, add 0.50 mL of each supernatant to 10 mL 3% nitric acid in a clean 50 mL tube. This is a 21-fold dilution.
- Prepare reagent blanks by adding 0.5 mL of each reagent to 10 mL 3% nitric acid in a clean 50 mL tube. For the aluminum solutions, add desired dose 400 µl 2:1 alum stock solution to 30 mL 0.1M NaOH, then add 0.5 mL of each dissolved aluminum solution to 10 mL 3% nitric acid.

C. Calculations

See Appendix C

APPENDIX C: Data analysis calculations

Raw data transferred into Excel.

1. Multiplied by 21 to account for dilution in 3% HNO_3
2. Multiplied by 0.03L to convert from ppb (µg/L) to µg element
3. Divided by the element molar mass and the original mass of dried sediment to convert from µg element to µmol/g
4. Multiplied by 8800 (percent solids x specific gravity of wet sediment x depth) and divided by 1000 to convert from µmol/g to mmol/m^2
5. Divided by 1E-6 (g/µg) and multiplied by the element molar mass times 1000 to convert from mmol/m^2 to g/m^2

APPENDIX D: Sequential extraction raw data for East Pond, Great Pond and China Lake

East Pond

(*Note: data was recorded prior to our current understanding of dithionite reaction parameters)

Sample	Extraction reagent	Alum dose, g/m2	[Al], g/m2	[Fe], g/m2	[P], g/m2
A	NH4Cl	0	0.01	0.01	0.01
	NH4Cl	4	0.03	0.44	0.01
	NH4Cl	7	0.01	0.00	0.00
	NH4Cl	15	0.03	0.00	0.00
	NH4Cl	29	0.04	-0.01	0.00
	Dithionite	0	0.03	30.64	0.97
	Dithionite	4	0.06	32.57	0.73
	Dithionite	7	0.09	33.75	0.59
	Dithionite	15	0.08	33.76	0.37
	Dithionite	29	0.04	32.00	0.17
	NaOH	0	19.46	1.52	5.60
	NaOH	4	21.44	1.31	5.56
	NaOH	7	22.05	1.28	5.70
	NaOH	15	26.18	1.26	5.81
	NaOH	29	32.64	1.21	6.09
B	NH4Cl	0	0.22	0.19	0.02
	NH4Cl	4	0.02	0.20	0.02
	NH4Cl	7	0.01	0.10	0.03
	NH4Cl	15	0.01	0.04	0.03
	NH4Cl	29	0.01	0.04	0.03
	NH4Cl	58	0.01	0.04	0.03
	Dithionite	0	0.33	19.39	0.49
	Dithionite	4	0.46	18.53	0.34
	Dithionite	7	1.01	18.14	0.29
	Dithionite	15	1.37	17.38	0.21
	Dithionite	29	0.75	16.86	0.10
	Dithionite	58	1.41	17.96	0.22
	NaOH	0	9.21	5.26	2.62
	NaOH	4	11.02	5.45	2.77
	NaOH	7	13.61	5.67	2.77
	NaOH	15	15.49	5.68	2.68
	NaOH	29	25.34	6.24	2.72
	NaOH	58	16.39	5.95	2.81
C	NH4Cl	0	0.01	0.04	0.01
	NH4Cl	4	0.01	0.07	0.01
	NH4Cl	7	0.00	0.04	0.02
	NH4Cl	15	0.01	0.04	0.02
	NH4Cl	29	0.00	0.03	0.01
	NH4Cl	58	0.02	0.02	0.01
	NH4Cl	15	0.01	0.03	0.01
	Dithionite	0	0.04	12.10	0.18
	Dithionite	4	0.02	7.72	0.16

	Dithionite	7	0.02	10.30	0.14
	Dithionite	15	0.04	9.82	0.12
	Dithionite	29	0.03	8.57	0.09
	Dithionite	58	0.02	0.02	0.01
	Dithionite	15	0.04	9.76	0.13
	NaOH	0	7.84	1.35	3.28
	NaOH	4	10.05	1.49	3.53
	NaOH	7	12.26	1.50	3.60
	NaOH	15	12.14	1.49	3.57
	NaOH	29	22.78	1.01	4.10
	NaOH	58	0.01	0.01	0.01
	NaOH	15	14.92	1.43	3.68
D	NH4Cl	0	0.00	0.03	0.02
	NH4Cl	4	0.00	0.03	0.02
	NH4Cl	7	0.00	0.04	0.02
	NH4Cl	15	0.01	0.32	0.02
	NH4Cl	29	0.01	0.03	0.02
	NH4Cl	58	0.01	0.04	0.03
	NH4Cl	15	0.00	0.02	0.02
	Dithionite	0	0.13	11.33	0.35
	Dithionite	4	0.27	11.05	0.21
	Dithionite	7	0.41	10.85	0.16
	Dithionite	15	0.23	10.30	0.09
	Dithionite	29	0.10	9.91	0.06
	Dithionite	58	0.09	12.96	0.06
	Dithionite	15	0.23	10.35	0.09
	NaOH	0	15.74	10.63	2.55
	NaOH	4	16.92	10.16	2.54
	NaOH	7	19.66	10.69	2.84
	NaOH	15	22.04	9.60	2.74
	NaOH	29	29.14	9.99	2.66
	NaOH	58	52.93	10.24	3.05
	NaOH	15	22.06	9.71	2.80
E	NH4Cl	0	-0.02	0.01	0.01
	NH4Cl	4	-0.03	0.00	0.02
	NH4Cl	7	0.03	0.55	0.04
	NH4Cl	15	-0.03	0.02	0.01
	NH4Cl	29	-0.02	0.17	0.02
	NH4Cl	58	0.02	0.23	0.06
	NH4Cl	15	-0.03	0.02	0.01
	Dithionite	0	0.26	2.53	0.17
	Dithionite	4	0.14	2.98	0.10
	Dithionite	7	0.06	2.74	0.07
	Dithionite	15	0.32	3.00	0.07
	Dithionite	29	0.49	3.12	0.07
	Dithionite	58	0.44	3.66	0.07
	Dithionite	15	0.45	3.91	0.09
	NaOH	0	8.28	2.35	2.14
	NaOH	4	11.18	2.35	2.25

	NaOH	7	12.44	2.39	2.23
	NaOH	15	17.18	2.51	2.24
	NaOH	29	28.34	3.77	2.19
	NaOH	58	52.63	6.53	2.24
	NaOH	15	17.12	2.50	2.20
F	NH4Cl	0	-0.03	-0.01	0.02
	NH4Cl	4	-0.03	-0.01	0.01
	NH4Cl	7	-0.03	0.00	0.01
	NH4Cl	15	-0.04	-0.02	0.01
	NH4Cl	29	-0.04	-0.02	0.01
	NH4Cl	58	-0.06	-0.05	0.01
	NH4Cl	15	-0.04	-0.02	0.01
	Dithionite	0	0.23	0.38	0.13
	Dithionite	4	0.19	0.35	0.09
	Dithionite	7	0.11	0.19	0.07
	Dithionite	15	0.13	0.17	0.05
	Dithionite	29	0.02	0.10	0.03
	Dithionite	58	-0.01	0.18	0.04
	Dithionite	15	0.12	0.16	0.04
	NaOH	0	11.18	3.27	2.53
	NaOH	4	13.32	3.19	2.63
	NaOH	7	13.70	3.01	2.49
	NaOH	15	18.81	3.09	2.45
	NaOH	29	27.32	3.31	2.44
	NaOH	58	50.57	4.64	2.51
	NaOH	15	19.68	3.25	2.52
G	NH4Cl	0	-0.02	0.03	0.01
	NH4Cl	4	-0.03	0.01	0.01
	NH4Cl	7	-0.03	-0.03	0.00
	NH4Cl	15	-0.03	-0.03	0.00
	NH4Cl	29	-0.03	-0.01	0.00
	NH4Cl	58	-0.06	-0.05	0.00
	NH4Cl	15	-0.03	-0.03	0.00
	Dithionite	0	0.27	36.15	0.55
	Dithionite	4	0.24	33.19	0.32
	Dithionite	7	0.27	22.16	0.11
	Dithionite	15	0.58	30.01	0.12
	Dithionite	29	0.31	27.12	0.05
	Dithionite	58	0.08	38.27	0.05
	Dithionite	15	0.63	31.22	0.14
	NaOH	0	11.38	11.59	2.38
	NaOH	4	13.16	11.41	2.43
	NaOH	7	15.93	12.29	2.53
	NaOH	15	18.07	12.10	2.76
	NaOH	29	-0.01	13.28	2.69
	NaOH	58	55.87	15.66	3.27
	NaOH	15	18.88	12.79	2.86
H	NH4Cl	0	-0.05	-0.04	0.01
	NH4Cl	4	-0.04	0.00	0.00

	NH4Cl	7	-0.04	-0.03	0.00
	NH4Cl	15	-0.03	-0.01	0.00
	NH4Cl	29	-0.03	-0.01	0.00
	NH4Cl	58	-0.04	-0.07	0.00
	NH4Cl	15	-0.02	0.04	0.00
	Dithionite	0	0.01	48.06	0.67
	Dithionite	4	0.08	42.63	0.37
	Dithionite	7	0.09	50.48	0.33
	Dithionite	15	0.10	47.67	0.21
	Dithionite	29	0.08	49.81	0.15
	Dithionite	58	0.03	54.81	0.13
	Dithionite	15	0.10	51.86	0.23
	NaOH	0	10.82	5.95	2.39
	NaOH	4	10.77	7.52	2.77
	NaOH	7	12.89	7.35	2.96
	NaOH	15	16.27	8.15	2.94
	NaOH	29	27.00	8.67	3.09
	NaOH	58	55.76	9.33	3.30
	NaOH	15	15.99	7.96	2.90
I	NH4Cl	0	-0.04	0.01	0.01
	NH4Cl	4	-0.05	-0.03	0.01
	NH4Cl	7	0.93	0.10	0.01
	NH4Cl	15	-0.03	0.00	0.00
	NH4Cl	7	-0.02	0.10	0.01
	Dithionite	0	0.02	46.77	0.62
	Dithionite	4	0.10	55.30	0.52
	Dithionite	7	0.15	55.88	0.26
	Dithionite	15	0.16	59.75	0.27
	Dithionite	7	0.16	57.41	0.36
	NaOH	0	0.13	48.58	0.22
	NaOH	4	17.08	6.56	2.96
	NaOH	7	22.72	8.00	3.29

Great Pond

Sample	Extraction reagent	Alum dose, g/m2	[Al], g/m2	[Fe], g/m2	[P], g/m2
A	NH4Cl	0	2.33	3.34	0.74
	NH4Cl	4	1.29	0.17	0.12
	NH4Cl	7	1.29	0.16	0.10
	NH4Cl	15	1.41	0.14	0.08
	NH4Cl	15	1.32	0.14	0.08
	NH4Cl	15	1.22	0.14	0.08
	NH4Cl	29	1.35	0.15	0.07
	NH4Cl	58	1.35	0.13	0.07
	BD	0	1.56	29.12	2.13
	BD	4	1.70	27.72	1.35
	BD	7	1.82	24.93	0.99
	BD	15	1.79	24.61	0.51

	BD	15	1.34	0.16	0.07
	BD	15	1.33	0.15	0.08
	BD	29	1.66	27.28	0.52
	BD	58	1.58	33.66	0.42
	NaOH	0	23.28	15.29	19.90
	NaOH	4	27.06	12.38	14.39
	NaOH	7	36.05	17.17	20.54
	NaOH	15	49.03	14.60	17.77
	NaOH	15	19.70	4.02	6.99
	NaOH	15	15.72	3.90	7.27
	NaOH	29	64.48	18.25	21.00
	NaOH	58	97.92	19.77	21.31

China Lake

Sample	Extraction reagent	Alum dose, g/m2	[Al], g/m2	[Fe], g/m2	[P], g/m2
A	NH4Cl	0	1.21	0.32	0.19
	NH4Cl	4	1.34	0.52	0.18
	NH4Cl	7	1.43	0.37	0.15
	NH4Cl	15	1.57	0.33	0.12
	NH4Cl	15	1.54	0.32	0.12
	NH4Cl	15	1.45	0.37	0.13
	NH4Cl	29	1.66	0.44	0.11
	NH4Cl	58	1.61	0.31	0.11
	Dithionite	0	1.40	81.53	4.94
	Dithionite	4	1.58	91.26	4.11
	Dithionite	7	1.51	84.73	2.29
	Dithionite	15	2.09	89.30	1.37
	Dithionite	15	2.84	106.79	1.14
	Dithionite	15	2.76	111.86	1.27
	Dithionite	29	3.13	101.23	1.03
	Dithionite	58	1.99	63.96	0.51
	NaOH	0	10.19	17.25	16.31
	NaOH	4	10.17	14.87	18.16
	NaOH	7	11.23	13.17	18.82
	NaOH	15	20.15	13.37	20.71
	NaOH	15	21.09	17.87	20.00
	NaOH	15	17.38	18.43	20.22
	NaOH	29	40.39	16.61	20.44
	NaOH	58	78.91	16.76	19.68
B	NH4Cl	0	1.58	1.06	0.20
	NH4Cl	4	1.42	0.39	0.15
	NH4Cl	7	1.39	0.45	0.13
	NH4Cl	15	1.51	0.45	0.11
	NH4Cl	15	1.47	0.37	0.11
	NH4Cl	15	1.54	0.39	0.13
	NH4Cl	29	1.52	0.31	0.10
	NH4Cl	58	1.53	0.23	0.09

	Dithionite	0	1.43	65.15	3.85
	Dithionite	4	1.48	68.40	1.33
	Dithionite	7	1.66	115.19	0.98
	Dithionite	15	1.69	73.78	0.64
	Dithionite	15	2.21	68.05	0.57
	Dithionite	15	1.42	133.96	0.57
	Dithionite	29	1.88	128.42	0.56
	Dithionite	58	1.41	90.34	0.31
	NaOH	0	0.66	4.12	0.81
	NaOH	4	0.68	4.12	0.65
	NaOH	7	1.01	4.01	0.62
	NaOH	15	2.56	5.52	0.76
	NaOH	15	2.34	3.94	0.62
	NaOH	15	-0.01	0.02	0.02
	NaOH	29	6.47	6.69	0.82
	NaOH	58	5.10	1.60	0.32
C	NH4Cl	0	0.27	0.06	0.22
	NH4Cl	4	0.26	0.10	0.04
	NH4Cl	7	0.25	0.07	0.02
	NH4Cl	15	0.42	0.16	0.03
	NH4Cl	15	0.36	0.10	0.02
	NH4Cl	15	0.34	0.05	0.02
	NH4Cl	29	0.45	0.10	0.02
	NH4Cl	58	0.49	0.08	0.02
	Dithionite	0	0.30	0.19	1.02
	Dithionite	4	0.26	0.10	0.10
	Dithionite	7	0.44	0.09	0.07
	Dithionite	15	0.52	0.09	0.05
	Dithionite	15	0.42	0.07	0.04
	Dithionite	15	0.53	0.08	0.05
	Dithionite	29	0.32	0.06	0.04
	Dithionite	58	0.34	0.06	0.03
	NaOH	0	1.32	1.16	2.07
	NaOH	4	1.76	1.08	0.79
	NaOH	7	2.73	0.96	0.52
	NaOH	15	5.38	0.95	0.41
	NaOH	15	7.93	1.33	0.62
	NaOH	15	5.58	1.11	0.39
	NaOH	29	15.76	1.39	0.47
	NaOH	58	29.79	1.56	0.45
D	NH4Cl	0	0.03	0.08	0.02
	NH4Cl	4	0.08	0.04	0.02
	NH4Cl	7	0.11	0.06	0.02
	NH4Cl	15	0.23	0.07	0.03
	NH4Cl	29	0.13	0.04	0.01
	NH4Cl	58	0.19	0.28	0.01
	Dithionite	0	0.15	49.30	1.30
	Dithionite	4	0.20	47.34	0.41
	Dithionite	7	0.21	51.94	0.36

	Dithionite	15	0.19	49.12	0.22
	Dithionite	29	0.13	43.55	0.12
	Dithionite	58	0.11	40.11	0.14
	NaOH	0	18.42	9.86	3.57
	NaOH	4	27.57	10.71	4.46
	NaOH	7	34.51	10.63	4.64
	NaOH	15	49.62	12.28	4.39
	NaOH	29	84.12	17.41	4.22
	NaOH	58	148.42	23.11	4.75
E	NH4Cl	0	5.21	7.33	0.15
	NH4Cl	4	3.81	5.87	0.13
	NH4Cl	7	3.53	3.37	0.08
	NH4Cl	15	3.64	2.98	0.08
	NH4Cl	29	5.90	2.84	0.07
	NH4Cl	58	9.63	2.11	0.06
	Dithionite	0	0.06	0.13	0.12
	Dithionite	4	0.21	0.09	0.08
	Dithionite	7	0.18	0.06	0.05
	Dithionite	15	0.18	0.07	0.04
	Dithionite	29	0.12	0.04	0.02
	Dithionite	58	0.10	0.04	0.02
	NaOH	0	17.03	7.48	3.01
	NaOH	4	18.26	4.98	2.78
	NaOH	7	37.33	6.98	3.14
	NaOH	15	38.33	6.87	3.21
	NaOH	29	56.94	7.01	2.93
	NaOH	58	73.25	7.19	2.82
G	NH4Cl	0	0.17	0.03	0.02
	NH4Cl	4	0.29	0.04	0.01
	NH4Cl	7	0.12	0.02	0.02
	NH4Cl	15	0.15	0.03	0.02
	NH4Cl	29	0.14	0.03	0.01
	NH4Cl	58	0.10	0.02	0.01
	Dithionite	0	0.48	50.78	0.86
	Dithionite	4	1.29	51.49	0.31
	Dithionite	7	0.69	56.07	0.21
	Dithionite	15	0.68	50.68	0.13
	Dithionite	29	0.50	50.75	0.07
	Dithionite	58	0.75	50.35	0.06
	NaOH	0	16.39	9.09	2.10
	NaOH	4	20.37	8.41	2.68
	NaOH	7	28.54	9.27	3.04
	NaOH	15	39.39	9.09	2.81
	NaOH	29	59.13	10.03	2.86
	NaOH	58	94.85	10.56	3.10

APPENDIX E: TGA raw data

First mass loss is mass of sediment lost upon heating to 100ºC. This is the fraction of water leaving the sediments.

Second mass loss is mass of sediment lost upon heating to 500ºC. This is the fraction of organic carbon leaving the sediments.

Sample name	Sample location	Initial mass (mg)	First mass loss (mg)	Second mass loss (mg)	Percent H2O	Percent C_{org}
A	44.46907, -69.51483	9.146	0.279	1.256	3.051	14.16
B	44.46273, -69.51888	33.986	0.852	3.749	2.507	11.31
C	44.45415, -69.52736	13.86	0.29	1.262	2.092	9.3
D	44.43878, -69.54225	21.099	0.366	1.448	1.735	6.98
E	44.43004, -69.54741	18.196	0.3	1.206	1.649	6.74
F	44.41805, -69.56328	15.83	0.227	0.981	1.434	6.29
G	44.40503, -69.57529	14.588	0.228	1.059	1.563	7.37